HHS Public Access

Author manuscript

Nat Cardiovasc Res. Author manuscript; available in PMC 2022 May 20.

Published in final edited form as:

Nat Cardiovasc Res. 2022 January ; 1(1): 67–84. doi:10.1038/s44161-021-00006-4.

Aortic intimal resident macrophages are essential for maintenance of the non-thrombogenic intravascular state

Gloria E. Hernandez[1,2], **Feiyang Ma**[1], **Guadalupe Martinez**[3], **Nadia B. Firozabadi**[2], **Jocelynda Salvador**[2], **Lih Jiin Juang**[4], **Jerry Leung**[4], **Peng Zhao**[5], **Diego A. López**[6], **Reza Ardehali**[5], **Anna E. Beaudin**[7], **Christian J. Kastrup**[4], **Matteo Pellegrini**[1,3], **Matthew J. Flick**[8], **M. Luisa Iruela-Arispe**[2,3,*]

[1]Molecular Biology Institute, University of California, Los Angeles, Los Angeles, CA 90095, USA.

[2]Department of Cell and Development Biology, Feinberg School of Medicine, Northwestern University, Chicago, IL 60611, USA

[3]Department of Molecular, Cell, and Developmental Biology, University of California, Los Angeles, Los Angeles, CA 90095, USA.

[4]Michael Smith Laboratories and Department of Biochemistry and Molecular Biology, University of British Columbia, 2185 East Mall, Vancouver, BC, V6T1Z4, Canada

[5]Department of Medicine, Division of Cardiology, University of California, Los Angeles, Los Angeles, CA 90095, USA.

[6]Department of Pathology, University of Utah School of Medicine, Salt Lake City, UT 84112

[7]Division of Hematology and Hematologic Malignancies, Department of Internal Medicine, University of Utah School of Medicine, Salt Lake City, UT 84112

[8]Department of Pathology and Laboratory Medicine, UNC Blood Research Center, University of North Carolina, Chapel Hill, Chapel Hill, NC 27599.

Abstract

Leukocytes and endothelial cells frequently cooperate to resolve inflammatory events. In most cases, these interactions are transient in nature and triggered by immunological insults. Here, we report that in areas of disturbed blood flow, aortic endothelial cells permanently and intimately

*Please address correspondence to: M. Luisa Iruela-Arispe, Ph.D., 303 E. Superior st. SQ 8-522, Northwestern University, Chicago, IL 60611, arispe@northwestern.edu - Phone: 312-503-7958.

CONTRIBUTIONS

GEH performed and designed experiments, wrote and edited the manuscript
GM, **NBF, JS** and **DAL** performed experiments and quantification
LJJ, JL, and **CJK** provided siRNA-nanoparticles
PZ performed the parabiosis experiments supervised by **RA**.
RA provided transgenic mice and provided intellectual input and discussion
AEB and **MF** provided key transgenic mice and provided intellectual input to experimental design and analysis.
MP provided intellectual input on experiments using single cell RNAseq data
FM performed bioinformatic analysis of scRNAseq data
MLIA conceived the study, designed the experiments, wrote and edited the manuscript
All authors discussed the results and had the opportunity to comment on the manuscript.

DECLARATION OF INTERESTS

CJK is a director and shareholder of NanoVation Therapeutics Inc., which is commercializing RNA-based therapies. All other authors declare no competing interests.

associate with a population of specialized macrophages that are recruited at birth from the closing ductus arteriosus and share the luminal surface with the endothelium becoming interwoven in the tunica intima. Anatomical changes that affect hemodynamics, like in patent ductus arteriosus, alter macrophage seeding to coincide with regions of disturbed flow. Aortic resident macrophages expand *in situ* via direct cell renewal. Induced-depletion of intimal macrophages led to thrombin-mediated endothelial cell contraction, progressive fibrin accumulation and formation of microthrombi that, once dislodged, caused blockade of vessels in several organs. Together the findings revealed that intravascular resident macrophages are essential to regulate thrombin activity and clear fibrin deposits in regions of disturbed blood flow.

Keywords

tissue-resident macrophages; shear stress; endothelial cells; heterotypic cell interactions

INTRODUCTION

As gatekeeper of the cellular traffic between blood and tissues, the endothelium is well equipped to interact with hematopoietic cells. Endothelial cells enable the well-coordinated process of diapedeses that includes, capture, rolling, and finally transmigration of leukocytes across the vascular barrier [1-4]. These events rely on complex and sequential molecular interactions whereby these cell types cooperate to mount and resolve inflammatory responses at the level of venules and capillaries [2,3]. In large arteries, interactions of the endothelium with inflammatory cells are mostly known for their association with atherosclerosis, a chronic inflammation of the vascular wall [5,6]. In this pathology, leukocytes occupy the subendothelial layer forming a neointima that progressively expands by the constant influx and local proliferation of inflammatory cells [5,7-9].

Other types of interactions between arterial endothelium and inflammatory cells have been shown, particularly a population of non-classical monocytes (Ly6C^{low}, CCR2^{low}, Cx3cr1^{high}) better referred to as patrolling monocytes that are thought to promote endothelial integrity and vascular health [10-12]. In addition to patrolling monocytes, myeloid cells with a highly dendritic appearance were also described in the luminal aspect of the aorta, especially at sites prone to develop atherosclerosis, like the aortic arch [13,14]. Despite their conspicuous location, the contribution of these myeloid cells to atherosclerosis was proved to be minimal, as their elimination only slightly delayed onset of the disease with no impact on duration or burden [15]. Thus, the mechanisms behind their peculiar distribution, specific seeding time and, more importantly, their function have remained puzzling.

Here we show that the emergence of aortic myeloid cells is not pathologically induced, instead it is developmentally triggered as part of natural hemodynamic changes at birth that result in localized disturbed flow dynamics. Genetic ablation of this aortic myeloid resident population promotes fibrin deposition and microthrombi formation, clarifying their function as critical regulators of hemostasis.

RESULTS

Alterations of hemodynamics associated with birth promote the seeding of myeloid cells in the tunica intima of the aorta

The fetal circulation includes two parallel circuits with equal left and right ventricular pressures. At birth, this balance changes drastically due to multiple concurrent events that include interruption of placental circulation, inflation of the lungs, and shift in pulmonary blood pressure. All these changes result in high left ventricular pressure and closure of the ductus arteriosus, a fetal vessel that connects the pulmonary arteries to the aorta, an event that further magnifies the oscillatory flow in the lower curvature of the aortic arch (Fig. 1a). These alterations in hemodynamics are quickly sensed by endothelial cells which respond to these flow changes transitioning from elongated to polygonal shape in the lesser curvature of the aortic arch (Fig. 1b,c). Furthermore, evaluation of mouse embryos and neonates uncovered a burst of inflammatory cells exiting from the constricted ductus arteriosus and that seed the aorta, in tandem with the changes in hemodynamics (Fig. 1d-f). Interestingly from the onset of birth, this population of CD45+ cells continued to reside in areas of the aorta that experience oscillatory/disturbed flow, including the lesser curvature of the aortic arch and branch openings (Fig. 1g-i, Supplementary Fig.1**a).** Initial characterization indicated that they also express CD11c (Fig. 1h,j). Curiously, CD11c+ cells were previously spotted in the aortic arch of adult healthy mice [13,14] raising the possibility that they might be the same population. We also found that CD11c+ cells progressively accumulate with age in the absence of pathologies or hypercholesterolemia (Supplementary Fig. 1**a-c**). However, they were not found in large veins, like the vena cava (Supplementary Fig. 1**d,e**), indicating that an arterial niche, including flow patterns may be required for their accumulation. Intimal immune cells were also absent from the carotids of healthy, adult mice (Supplementary Fig. 1**f**) and from the descending young aorta, except for branches (Supplementary Fig. 1**g**). We also observed that the distribution of these cells progressively broadened with age. In fact, the descending aorta of 52- and 78-week-old mice revealed ongoing accumulation of intimal immune cells even in areas of laminar flow (Supplementary Fig. 1**g-i**). These findings suggested underlying requirements for intimal myeloid cells seeding that although initially associated with oscillatory/disturbed flow, might also be tied to vascular aging.

A definitive link between onset of oscillatory flow and recruitment of CD11c+ cells was established using mouse models of patent ductus arteriosus (PDA). Failure in PDA closure significantly alters cardiovascular hemodynamics[16]. While viable and fertile [17], *Vimentin*$^{-/-}$ mice exhibit PDA in about 88% of adults, making them an ideal model to study myeloid cell distribution in adult aortae [18]. At 10wks of age, the ductus arteriosus in wild-type littermates becomes a solid fibrous structure that persists as the ligamentum arteriosum (Fig. 1k). In contrast, *Vimentin*$^{-/-}$ mice exhibit a viable ductus arteriosus which impacts patterns of disturbed flow distribution and the location of myeloid cells (Fig. 1l). The lesser curvature of the aortic arch of Vimentin$^{-/-}$ mice showed no intimal myeloid accumulation, instead myeloid cells were noted surrounding the openings of the ductus arteriosus, subclavian artery, and onset of the descending aorta (Fig. 1l).

The thin nature of the endothelial lining makes it difficult to ascertain the precise topological location of myeloid cells in relation to the endothelium. Thus, we performed 3D surface rendering using *CDH5*^{creERT2}*;R26*^{tdtomato} reporter mice to label the endothelial monolayer tdTomato. Aortae were stained with CD45 and VE-cadherin in order to generate 3D depiction of the tunica intima. Surprisingly, intimal myeloid cells were neither above nor below the endothelium, but were instead interwoven within the endothelial monolayer with some immune cell processes projecting into and others below the lumen (Fig. 2a). *En face* scanning electron microscopy of the aortic arch stained with CD45 antibodies confirmed these findings (Fig. 2b). Additionally, 3D surface rendering using a reporter model that labels the tunica media (*SM22*^{cre}*;R26*^{tdTomato}) revealed that these aortic immune cells were in fact located in the tunica intima, as per location within the VE-Cadherin stained layer (Fig. 2c). Finally, exposure of myeloid cells into the vascular lumen was additionally supported by injection of CD45 antibodies *in vivo* (Fig. 2d,e).

It has been previously reported that during transendothelial cell migration, leukocytes express Pecam-1 in order to adhere to the endothelial cells and therefore, preserve junctional integrity while crossing the endothelial barrier [2-4]. Interestingly, *en face* images showed Pecam-1 protein expression, suggesting that Mac^{AIRs} could bind to the endothelium via homophylic-heterotypic interactions and to prevent barrier disruption (Fig. 2f). To uncover if the Pecam-1+ regions were lumen facing or beneath the endothelial cells, we injected non-blocking Pecam-1 (390) antibody intravenously. *En face* images revealed Pecam-1+ regions in the cell bodies of inflammatory cells exposed to the lumen (Fig. 2g). Combined, these experiments revealed that in regions of oscillatory and disturbed flow the constituency of the endothelial layer is enriched by a population of myeloid cells that intimately co-exists with the endothelium in the absence of pathology and without breach of permeability.

scRNA-seq reveals the transcriptional identity of the aortic intimal immune cells

In order to recover cellular identities independent of defined labeling strategies, we turned to single-cell RNA sequencing (scRNA-seq) using specimens that were not FACS-sorted. We previously developed a unique isolation strategy that allows us to collect cells from the tunica intima avoiding prolonged enzymatic digestion or staging cells in suspension[19,20] (Supplementary Fig. 2**a**). Using this approach, we made 3 independent scRNA-seq libraries, capitalizing on regions containing an abundant number of intimal immune cells. Thus, we harvested intimal cells from the aortic arch of 8wk old C57BL/6 mice (**“**Young Arch”) and from the descending aorta (thoracic and abdominal portions) of 78wk C57BL/6 old mice (**“**Aged Descending A,B”), where each library contained 6-8 aortae (Supplementary Fig. 2**b-e**; Supplementary Table 1). Comparisons between these groups would allow us to ascertain whether cells in young mice in areas of disturbed flow resemble those in laminar flow in aged mice. Using dimensionality reduction by the t-distributed stochastic neighbor embedding (t-SNE) analysis, we identified 10 distinct cell types and assigned cellular identities (Supplementary Figure 2**f;** Supplementary Table 2,3) based on canonical lineage markers (Supplementary Figures 2**g and** 2**h**). Within the 10 cell types, we identified two distinct macrophage populations based on *Fcgr1* (CD64) and *Adgre1* (F4/80) expression (Supplementary Figures 2**h**), which we suspected to include the intimal immune cells. One of the macrophage populations highly expressed *Lyve1* (lymphatic endothelium hyaluronan

receptor-1), *F13a1*, and *Mrc1* (CD206), well-known markers of adventitia macrophages [15,21-24] (Supplementary Fig. 2**i,j**), suggesting this macrophage population came from the adventitia. While our isolation method enriches for cells in the tunica intima, few cells from the other aortic layers (tunica adventitia and media) were also captured[19,20] (Supplementary Fig. 2**f and** 2**g**). Therefore, we predicted that one of the two macrophage populations identified was from the adventitia. To definitively test this prediction, we performed single cell sequencing from dissected aortic adventitia (**Supplementary Fig. 3a-g)** and compared the two distinct myeloid populations identified. For this, we selected the CD14 positive cells from the purified adventitia and intimal-enriched libraries (**Supplementary Fig. 3c-e)** and were able to discern two clear clusters of macrophages from the aorta: a Lyve1 positive/CD64 group of cells which was also present in the libraries from the adventitia and clearly related to typical adventitial macrophages and a second cluster that showed distinct expression of Mmp12 and Mmp13 (**Supplementary Fig. 3f,g)** which was unique to the intima-enriched aortic libraries and absent from the adventitia. Furthermore, we compared the Mmp12/13 aortic macrophage population with macrophages in the Tabula muris atlas[25] (**Supplementary Fig. 4a-h**) and resident macrophages characterized in more recent publications[22] (**Supplementary Fig. 4i**). From this analysis, it became clear that the aortic population of intimal macrophages was especially distinct from resident macrophage populations present in other organs to date, apart from sympathetic nerve-associated macrophages found in the lung[22]. Amongst the unique transcriptional markers for intimal macrophages, MMP12 and MMP13 were the most distinctive transcripts.

Subsequently, we compared the Mmp12 and Mmp13 macrophage population to a recently identified group of macrophages isolated from whole aortas and referred to as Mac^{AIRs} [15]. Comparisons between the intimal Mmp12/13+ population presented here to the pre-hypercholesterolemic aortic Mac^{AIRs} population[15] revealed that they were transcriptionally identical (Supplementary Table 4). Interestingly, we also found that the young arch and old thoracic endothelial-associated macrophage populations were identical (**Supplementary Figure 4j**; Supplementary Table 5), suggesting the endothelial niche is responsible for the underlying tissue-specific imprinting of these macrophages, no matter age or location. This realization prompted two immediate questions: Were these populations progeny of the CD45+ cells exiting the ductus arteriosus? And, more importantly, what was their biological relevance?

Aortic intima resident macrophages (Mac^{AIRs}) are a distinct macrophage population that seeds the aorta at birth

In order to clarify the function of Mac^{AIRs} and delve into their developmental origin, we first performed differential expression analysis to seek as many unique markers as possible. As per direct comparisons with adventitial macrophages and Tabular muris atlas, we found that Mac^{AIRs} expressed significantly higher transcriptional levels of matrix metalloproteinases (*Mmp12, Mmp13*; Supplementary Fig. 2**i,j**) and exhibited increased expression of immune cell activation genes (*Il1b*, *Ccl3*, *Ccl4*, *Tnf*, *Cxcl2*, *Cxcl16*; Supplementary Fig. 2**i,j;** Supplementary Table 6-8). In addition, Mac^{AIRs} displayed genes involved with wound healing / identification of dying cells (*Axl*, *Tyrobp*, *CD44*, *CD74*; Supplementary Fig. 2**i,j;** Supplementary Table 6-8) and showed higher expression levels of antigen presenting

genes, such as major histocompatibility complex class II (MHC class II) encoding genes (*H2-Aa*, *H2-Ab1*, *H2-Eb1*, and *H2-M2*; Supplementary Fig. 2**i,j;** Supplementary Table 6-8). In contrast, adventitia *Lyve1*^{hi} macrophages expressed genes associated with M2-like macrophages *(F13a1, Folr2* and *Mrc1 (CD206))*; Supplementary Fig. 2**i,j**; Supplementary Table 7,8).

To match the expression profile to their presumed progenitors, immunohistochemistry was performed on aortae of P7 and adult mice for targets unique to Mac^{AIRs} (Mmp13, Cxcl16, and CD11c). Intimal CD45+ cells colocalized with Mac^{AIR} markers (**Supplementary Fig. 5a,b**) whereas, in the adventitia, no CD45+ cells showed expression of Mac^{AIR} markers (**Supplementary Fig. 5c**). We also found that Mac^{AIRs} expressed Cx3cr1 (fractalkine receptor) transcripts (**Supplementary Fig. 5d**) and protein (**Supplementary Fig. 5e**). Moreover, using an inducible Cx3cr1 reporter model (*Cx3cr1*^{creERT2};*R26*^{tdTomato}), 98% of all intimal CD45+ cells in adult aortae were labeled tdTomato (**Supplementary Fig. 5f**), which also colocalized with Cxcl16 protein expression (**Supplementary Fig. 5g**); thus, demonstrating the activity of the *Cx3cr1* promoter, which was later used in lineage tracing analysis. Additionally, using this transgene, intimal CD45+ cells in P5 aortae were also labeled by the reporter post- tamoxifen treatment (P1 and P3), further indicating that Mac^{AIRs} seed the aorta immediately post-birth (**Supplementary Fig. 5h**). Overall, these findings support the conclusion that the immune cells accumulating and residing in the tunica intima after birth were Mac^{AIRs} progenitors.

To more definitively confirm origin and the macrophage identity of Mac^{AIRs} (versus dendritic cells (DCs)), we assessed recombination labeling using the *Csf1r*^{MerCreMer};*R26*^{tdTomato} macrophage fate-mapping model. In this transgenic model, we found all intimal immune cells (CD45+) to also be labeled by the reporter gene tdTomato (**Supplementary Fig. 5i**). Moreover, all intimal immune cells expressed CD68 protein (**Supplementary Fig. 5j**). Additionally, Mac^{AIRs} did not express DC master regulator transcription factor *Zbtb46* [26] nor classical DC markers *CD8a, Ccr7* (**Supplementary Fig. 5k**), *CD103*, *33D1*, or *Mycl* (data not shown, genes not detected in dataset). Furthermore, Mac^{AIRs} were shown to phagocytose dying (annexin +) endothelial cells *in vivo* (**Supplementary Fig. 5l**), providing functional evidence of their macrophage identity. Thus, Mac^{AIRs} are a transcriptionally unique macrophage population that takes residency in the tunica intima of the aorta shortly after birth in regions of oscillatory and disturbed flow.

Mac^{AIRs} are self-maintained throughout adulthood

It is now understood that many tissue-resident macrophages are maintained through self-renewal without contribution from circulating monocytes[27,28]. EdU incorporation assays showed that in a 2h pulse, 5.4% of Mac^{AIRs} were undergoing DNA replication *in situ* in the adult arch (**Supplementary Fig. 6a-c**), suggesting that Mac^{AIRs} followed the trend of other resident macrophages. Long-term replenishment was assessed by lineage tracing with pulse-labeling *Cx3cr1*^{creERT2};*R26*^{tdTomato} mice and evaluation 10- and 20- wks post-labeling (**Supplementary Figures 6d,e**). To control for the possible contribution of circulating cells using this model, we also quantified levels of tdTomato positive circulating cells. FACS analyses indicated that after 3wks, CD45+ tdTomato+ peripheral blood was negligible (less

than 0.5%; **Supplementary Fig. 6f,g**) and thus, negating the possibility that cells from the circulation contributed to reporter positive Mac^{AIRs} after 20-wks post-tamoxifen. In this manner, absence of circulating tdTomato+ cells allowed us to ask whether monocytes participated in the maintenance of Mac^{AIRs}. Although the labeling frequency of Mac^{AIRs} decreased by 10% after 10-wks post-tamoxifen injection, we noted that reporter expression remained constant for an additional 10wks (20wks total) (**Supplementary Fig. 6e,h**). This finding supports the conclusion of local self-renewal with negligible contribution from circulating monocytes.

To further confirm these findings, we performed parabiosis experiments using adult GFP+ and wild-type (WT) mice. As follows, both mice shared a chimeric circulation for 5-wks (**Supplementary Fig. 6i**). The experiment allowed for all circulating cells to access the aortic regions of interest (i.e. the lesser curvature). The presence of GFP+ intimal immune cells incorporated in the WT mice would infer monocyte contribution and vice versa (**Supplementary Fig.6i**). Additionally, we only used mice with efficient parabiosis, which was confirmed by examining the chimerism of CD45+ peripheral blood cells (**Supplementary Fig. 6j**). Evaluation of the lesser aortic curvature in the WT mice revealed no GFP+ intimal immune cells (**Supplementary Fig. 6k**), proving further strength to the conclusion that Mac^{AIRs} maintenance was independent of circulating monocytes. This conclusion was further strengthened by clonal analysis of an inducible multicolor fluorescent labeling model (*Cx3cr1*^{creERT2};*R26*^{Rainbow}) whereby expression of cre-recombinase in cells expressing Cx3cr1 would randomly recombine given rise to three possible colors (**Supplementary Fig. 6l**). Here labeling was done at 8 weeks and clonal expansion evaluated 9 months later (at 11months). The data strongly argues that Mac^{AIRs} are self-maintained.

Mac^{AIRs} are the progeny of definitive hematopoietic cells that exit the ductus arteriosus at birth and expand through self-renewal

Mac^{AIRs} colonize the aorta as they exit from the ductus arteriosus and migrate to areas of disturbed flow. After this initial wave of migration, Mac^{AIRs} expand in number by local proliferation (Figure 3a). Nonetheless, lineage tracing was required to fully ascertain adult progeny. Thus, we performed lineage analysis using the inducible *Cx3cr1*^{creERT2};*R26*^{tdTomato} reporter model to label Mac^{AIRs} immediately post-birth and follow their descendants over time (Figures 3b,c). Using this model, 63% of intimal CD45+ cells were tdTomato positive at P7 after administration of tamoxifen after birth. By 4wks we found 91% of intimal CD45+ cells in aortae retained the tdTomato labeling (Fig. 3d-f). We interpret the increase from P7 (63%) to 4wks (91%) to indicate that only those inflammatory cells expressing Cx3cr1 were successfully retained in the endothelium. Importantly, at 4wks of age less than 0.5% of peripheral blood cells were tdTomato positive (Fig. 3f), supporting the absence of contributions from circulating cells. Therefore, these data indicate that the Mac^{AIRs} that enter the aorta postnatally expand via self-renewal and colonize the lesser curvature of the aortic arch with minimal (if any) input from circulating monocytes.

To assess clonal expansion of the Mac^{AIRs} at early time-points, we again used the inducible *Cx3cr1*^{creERT2};*R26*^{Rainbow} model to ascertain clonality and tracing (Fig. 3g). Using this

model, pups were treated with tamoxifen immediately post-birth to induce stochastic genetic recombination yielding permanent expression of up to three mutually exclusive fluorescent protein labels: Cerulean, mOrange, and mCherry (Fig. 3g). At 8wks of age, we observed clones of labeled Mac^{AIRs} in the aortic arch (Fig. 3h), confirming Mac^{AIRs} self-expand *in situ* after seeding the aorta immediately post-birth. We also examined Mac^{AIRs} levels in chemokine receptor *2*-deficient (*CCR2*−/−) mice, where Ly6C^{hi} (classical) monocyte emigration from the bone marrow is defective [29]. Compared to control mice, we found no difference in the proportion and number of intimal CD11c+CD45+ (Mac^{AIRs}) cells in the aortae of either young (P7) or adult (8wk) mice (Fig. 3i,j). This further solidifies the notion that postnatal aortic intimal macrophages self-expand and maintain their population independently of circulating monocytes at steady-state (Fig. 3k).

Assessment as to whether Mac^{AIRs} were derived from primitive or definitive hematopoiesis lineages was determined through experiments with a defined lineage tracing model (*Flt3*^{cre};*R26*^{mTmG}) that labels cells arising from definitive hematopoietic stem cells as GFP+ [27,30,31] (**Supplementary Fig. 6m**). P5 aortae from *Flt3*^{cre};*R26*^{mTmG} mice showed that a large proportion of intimal CD45+ cells were GFP+ relative to circulating CD11b^{hi}Gr1^{lo} monocytes (**Supplementary Fig. 6n,o**). The recombination labeling, combined with the observation that these macrophages were not detected until after birth, strongly indicates that these cells were derived from definitive hematopoiesis lineage and not from the yolk sac, as is known to occur for some resident macrophage populations[27,28].

Mac^{AIRs} blunt thrombin activity in areas of oscillatory flow

An inducible diphtheria toxin model (*Cx3cr1*^{creERT2}*;CSF1R-flox-stop-flox-DTR*) whereby dual tamoxifen and diphtheria toxin (DTx) injections result in elimination of cells expressing both Cx3cr1 and CSF1R was used to deplete Mac^{AIRs} and clarify their biological relevance (Fig. 4a). Efficient loss of Mac^{AIRs} was noted 24hrs post-DTx injection (Fig. 4b) and was associated with altered endothelial morphology and apparent reduction of cell size (Fig. 4c, **Supplementary Fig. 7a**). To clarify whether this was related to actual endothelial contraction, we evaluated the expression of phospho-myosin light chain 2 (pMLC2). In control mice, Mac^{AIRs} showed high expression of pMLC2 (Fig. 4d, **Supplementary Fig.7b**). Upon Mac^{AIR} depletion, endothelial cells became positive for pMCL2 indicating a highly contractile functional state, likely the reason behind the drastic change in cell size (Fig. 4c-d, **Supplementary Fig. 7b**). Together, these findings suggested that Mac^{AIRs} prevented a contractile phenotype in the endothelium which would otherwise manifest in areas of oscillatory/disturb flow through an unclear mechanism.

It is well-known, that exposure of cultured endothelial cells to thrombin, results in rapid Rho activation, phosphorylation of MLC2, stress fiber formation, contraction, and disruption of endothelial junctions [32,33] (**Supplementary Fig. 7c**). All of these events are triggered downstream signaling by GPCR protease-activated receptor 1 (PAR1), a receptor highly expressed by aortic endothelial cells (**Supplementary Fig. 7d**), and activated upon cleavage by thrombin[32,33]. Interestingly, plasmin and other proteases, including MMP12 and 13 both highly expressed by Mac^{AIRs} (Figure 4e), can alter this signaling pathway by cleaving PAR receptors that are carboxyl-terminal to the thrombin cleavage site and thus, prevent

thrombin-mediated endothelial contraction[34-37]. Consequently, we posit that in absence of Mac^{AIRs}, intact endothelial PAR1 was available to be activated by thrombin leading to endothelial contraction. This assumption implied accumulation of thrombin in areas of oscillatory/disturbed flow. Indeed, staining for thrombin revealed presence of thrombin at the lesser curvature of the aortic arch and branch openings (Fig. 4f). Additionally, to further confirm the thrombin activity in regions of disturbed flow, we treated control or *Cx3cr1*^{creERT2};*CSF1R*^{flfDTR} mice with Vehicle or Dabigatran (thrombin-specific inhibitor) and assessed endothelial cell contraction (Fig. 4g). Five days post-treatment, dabigatran-control mice still expressed pMLC2 in Mac^{AIRs}, indicating that macrophage contraction was thrombin-independent (Fig. 4h). However, depletion of m Mac^{AIRs} with concurrent dabigatran treatment prevented endothelial cell contraction, as per pMLC2 expression and cell size quantification (Fig. 4h,i), demonstrating that endothelial cell contraction was thrombin-dependent, but mitigated when Mac^{AIRs} were present. Thrombin was still present in areas of oscillatory flow after macrophage depletion (**Supplementary Fig. 7e**). Together, these findings indicate Mac^{AIRs} prevent endothelial contraction driven by thrombin in regions of oscillatory flow. Importantly, we tested other aspects of clotting in the presence and absence of macrophages, including tail bleed times (**Supplementary Fig. 7f**); as well as other mediators / regulators of the clotting such as nitric oxide and prostacyclin (**Supplementary Fig. 7g,h**). None of these were altered by deletion of Mac^{AIRs}.

The next critical question was to sort out the molecular mechanism whereby Mac^{AIRs} impaired thrombin action, and in particular pMLC2, in endothelial cells. It is well accepted that thrombin mediates signals on endothelial cells through protease activated receptors (PAR1, 2 and 4) [32,33], all expressed by aortic endothelial cells, but not by Mac^{AIRs} (**Supplementary Fig. 7d**). Interestingly PAR receptors can be cleaved by thrombin, mediating signaling, but also by other proteases like Mmp12 and Mmp13 blunting these signals by cleaving PAR1 upstream the thrombin site[34-37]. Considering the high levels of Mmp12 and 13 expressed by Mac^{AIRs} it was only logical to fill the dots and predict that matrix metalloproteases secreted by Mac^{AIRs} impaired thrombin-mediated contraction in endothelial cells. While testing this hypothesis in mouse aorta was impossible, we evaluated thrombin signaling, as per pMLC2 levels on endothelial cells in the presence and absence of Mmp13 (Figure 4j). The findings, presented in Figure 4j clearly shows that thrombin activates pMLC2 in the endothelium and that this effect is impaired by co-incubation with Mmp13.

Mac^{AIRs} residency coincides with deposition of fibrin(ogen)

The presence of thrombin in areas of disturbed flow led us to inquire whether fibrinogen, a substrate of thrombin, was also found in these regions. Indeed, *en face* staining for fibrin(ogen) in the arch of 8wk old C57BL/6 mice revealed the buildup of fibrin(ogen) in the lesser curvature (Fig. 5a). Higher magnification images (Fig. 5b) and 3D surface rendering (Fig. 5c) also revealed that fibrin(ogen) decorated the surface of Mac^{AIRs}. To further confirm that fibrin(ogen) is deposited in regions of disturbed flow, we depleted endogenous fibrinogen *in vivo* and then treated those mice with fluorescently tagged fibrinogen to assess binding sites and accumulation (Fig. 5d). Knock-down of fibrinogen was accomplished by delivery of siRNA targeting hepatic fibrinogen mRNA (siFibrinogen),

which was encapsulated in lipid nanoparticles containing an ionizable cationic lipid[38]. At 7d post-treatment circulating fibrinogen was ~90% depleted (Fig. 5e) and at this time, fibrinogen-a488 (fbg-a488) 3-hours post-injection bound avidly to Mac^{AIRs} and accumulated throughout lesser curvature (Fig. 5f). In contrast, Fbg-a488 did not accumulate in the greater curvature (**Supplementary Fig. 8a**), confirming the predilection of fibrinogen accumulation in regions of disturbed flow.

We validated concurrent associations of Mac^{AIRs} and fibrin(ogen) in intercostal artery openings (Fig. 5g). The correlation was also noted in 78wk old descending aortae (**Supplementary Fig. 8b**). Moreover, a time course evaluation showed progressive fibrin(ogen) accumulation in the aortic arch of P7, 3wk, and 8wk mice coinciding with the expansion of Mac^{AIRs} with age (**Supplementary Fig. 8c**). As fibrinogen is a substrate for macrophages, we predicted that fibrinogen deposits might be required for seeding of Mac^{AIRs} in the regions of disturbed flow in the tunica intima. Thus, we analyzed Mac^{AIR} accumulation in fibrinogen-deficient mice (*Fbg*$^{-/-}$) [39] and in mice expressing a mutant form of fibrinogen that could not be converted to fibrin polymer (*Fbg*^{AEK}) [40]. Our prediction was incorrect as no difference in the abundance or distribution of Mac^{AIRs} was found in either mouse model (Fig. 5h). These findings reconcile that while overlapping in location, fibrin(ogen) was dispensable for the seeding or anchoring Mac^{AIRs} to the tunica intima.

Mac^{AIRs} are necessary to clear fibrin(ogen) deposits in regions of disturbed flow

The concurrent presence of both thrombin and fibrin(ogen) in areas of disturbed flow implied that Mac^{AIRs} might be involved in preventing fibrin formation; therefore, we explored fibrin(ogen) accumulation in the *Cx3cr1*^{creERT2};*CSF1R*^{flfDTR} model over time (Fig. 6a). Evaluation of fibrin(ogen) levels at 7- and 14-days post-continued depletion revealed progressive and significant accumulation in the lesser curvature (Fig. 6b-d, **Supplementary Fig. 8d**). Additionally, fibrin fibrils were clearly visible in the 14-day macrophage-depleted aortae (Fig. 6c), which were never detected in control mice. The data implies that Mac^{AIRs} promote clearance of fibrin(ogen) and/or prevention of fibrin formation. Further, *en face* aortae SEM images (Fig 6e, **Supplementary Fig. 8e**) revealed microthrombi and polymerized fibrin decorating the lesser curvature of *Cx3cr1*^{creERT2};*CSF1R*^{flfDTR} mice but not in littermate controls. Microthrombi were also noted by confocal microscopy along with rupture of the endothelial lining (Fig. 6f,g). As a direct read-out of disseminated microthrombi, we evaluated D-dimer and found markedly elevated levels in macrophage-depleted mice compared to undetectable levels in control mice (Fig. 6h), further supporting hemostatic imbalance. Histological examination of tissues from Mac^{AIR} depleted mice revealed hemorrhagic foci in multiple tissues, including kidney, liver, and lung (Fig. 6i). Images of the kidneys from *Cx3cr1*^{creERT2}; *CSF1R*^{flfDTR} mice that had to be euthanized due to health decline exhibited diffused and abundant fibrin(ogen) throughout the tissue (Fig. 6j), consistent with vascular rupture. Based on the data presented, it is likely that dislodged microthrombi traveling through the circulation were responsible for occluding smaller diameter vessels leading to hemorrhagic foci and organ damage. Additional support to the requirement of Mac^{AIRs} in clearing fibrin(ogen) deposits, also emerged from evaluation of CD11c−/− mice. Absence of CD11c results in a significant reduction in the number of Mac^{AIRs}, indicating that that

CD11c was necessary, albeit not fully sufficient for anchorage of Mac^{AIRs} to the intimal niche as could still detect some macrophages (approximately 45% in comparison to controls) in the tunica intima of this mouse. Importantly, this mouse model also exhibited an impressive accumulation of fibrin(ogen) (**Supplementary Fig.8f**). An alternative explanation for fibrin(ogen) accumulation and thrombosis upon Mac^{AIRs} depletion could relate to break of barrier integrity in areas of oscillatory flow; implicating Mac^{AIRs} in the maintenance of endothelial junctional integrity in those areas. We tested this possibility by examining fluorescent microspheres (40nm) deposition in the tunica intima of littermate control and *Cx3cr1*^{creERT2};*CSF1R*^{flfDTR} mice that both received tamoxifen and diphtheria toxin injections (1-day Mac^{AIR} depletion) (**Supplementary Fig. 8g**). While the positive control (buffered EDTA intracardiac injection for (5min)) resulted in robust deposition of fluorescent beads in between cells, no accumulation fluorescent beads was found in any of the other groups (**Supplementary Fig. 8g**). Thus, Mac^{AIRs} do not play a role in maintaining barrier integrity, instead appear to necessary to clear fibrin(ogen) deposits and mitigate PAR1-thrombin signaling in regions of disturbed flow.

The drastic phenotype observed from depletion of Mac^{AIRs}, a relatively small cell population, prompted the question as to whether the experimental approach might alter a broader group of macrophages. Thus, we evaluated alterations in the macrophage populations of multiple organs by FACs analysis (Fig. 6k). The findings revealed that while bone marrow and peripheral blood were affected by the dosage of tamoxifen/diphtheria toxin used, none of the other Cx3cr1+Csf1r+ macrophage populations in the evaluated organs were altered. The implication is that areas of oscillatory/disturbed flow in the arterial tree are sites of fibrin accumulation that absolutely depends on Mac^{AIRs} for clearance with critical consequences. A few last important pieces of evidence to solidify this conclusion were still pending, including how do Mac^{AIRs} degrade fibrin(ogen)?

Macrophages have been known to express plasminogen receptors to degrade fibrin(ogen) extracellularly[41]. Importantly, Mac^{AIRs} expressed plasminogen receptors (Fig. 6l) and bound to fluorescently conjugated plasminogen when intravenously injected (Fig. 6m). Thus, in addition to MMP12 and 13, Mac^{AIRs} are capable of generating cell surface-associated plasmin particularly with the aid of endothelial cells, which express high levels of tissue-type plasminogen activator (**Supplementary Fig. 8h,i**). We also confirmed that neither endothelial cells nor Mac^{AIRs} expressed plasminogen (**Supplementary Fig. 8j**). Taken together, our findings indicate that Mac^{AIRs} are required to clear fibrin(ogen) deposits, prevent fibrin formation and maintain an anti-thrombotic state in areas of disturbed flow.

Additional support to the conclusion that Mac^{AIRs} are responsible for clearing fibrin(ogen) deposits in regions of disturbed flow came from experiments whereby Mac^{AIRs} were allowed to return after a 2 week depletion. Much like resident macrophages in other organs[27,28,42-44], we found that upon removal of Mac^{AIRs} and elimination of depletion pressure (tamoxifen and diphtheria toxin), monocytes seed areas of disturbed flow and reconstitute the Mac^{AIR} population (Figure 7a-d). A gradual increase of macrophage number was demonstrated after evaluation of the aorta of mice at 1wk and 2wk post-depletion (Figure 7d). Importantly, increase of Mac^{AIR} was associated with reduction of the accumulated fibrin(ogen) (Fig. 7c,e). Moreover, circulating D-dimer levels (Fig. 7f) and

endothelial cell size in the lesser curvature of the aorta (Fig. 7g) also returned to control levels. Overall, these findings further support the conclusion that Mac^{AIRs} are required clear fibrin(ogen) deposits in regions of oscillatory and disturbed flow.

DISCUSSION

Vascular endothelial and hematopoietic cells are well-known to coordinate inflammatory responses. Here, we have expanded these functions to also include regulation of intravascular hemostasis. Indeed, our findings indicate that while endothelial cells provide a non-thrombogenic surface facilitating blood circulation, in areas of oscillatory or disturbed flow, this function is challenged by the accumulation of fibrinogen and thrombin (aortic arch and branches with rapid flow). In these regions, the presence of a population of intima resident macrophages (Mac^{AIRs}), summoned to areas of disturbed flow from birth, is critical to effectively clear fibrinogen and prevent intravascular clotting.

Macrophage association with the endothelium is not necessarily surprising, and when seen in aortic tissue sections, the assumption is that this heterotypic interaction might be part of an inflammatory or pre-atherosclerotic lesion. However, the unusual feature that captured our attention was the highly reproducible seeding of this macrophage population post-birth and their unique topology in relation to the endothelium. These elements indicated that seeding of these macrophages in the luminal aspect of the aorta was not part of an inflammatory response; instead, the process was a normal developmental program by which Mac^{AIRs} become a constitutive component of the tunica intima in regions of oscillatory and disturbed flow. While the work presented here addressed multiple points related to origin, lineage, and self-renewal, why are these cells attracted to areas of disturbed and oscillatory flow; how and why do they migrate from the closing ductus arteriosus to those regions are important questions that remain unanswered. A logical assumption is that disturbed flow alters the endothelium creating unique niche conditions that attract monocytes to those sites and promote Mac^{AIRs} differentiation into a stable population capable of self-renewal. While the characterization of the endothelial niche remains unclear, we predict that thrombin is likely a requirement, as per the presence of this enzyme in regions of oscillatory and disturbed flow.

The ability of macrophages to cleave fibrinogen and participate in the remodeling of the provisional matrix formed during wound healing has been established long ago[45]. This being said, the repertoire of proteases is distinct in different macrophage subtypes, some proteases being expressed only upon induction and in situations of wound healing. We found that unlike adventitial and other macrophage populations, Mac^{AIRs} constitutively express MMP12 and MMP13, known to cleave fibrinogen[46-48]. In addition, Mac^{AIRs} also bind to plasminogen and this anchorage enables endothelial tPA to generate plasmin, which also degrades fibrinogen and fibrin. Together, this repertoire of proteases enables intravascular macrophages to efficiently remove fibrinogen deposits and antagonize fibrin accumulation driven by procoagulant pathways and the presence of thrombin in areas of oscillatory/disturbed flow. Furthermore, MMP-12 and −13 also cleave the protease activating receptor-1 (PAR-1) preventing its activation by thrombin[34-37]. Highly expressed by endothelial cells, PAR-1 promotes Rho activation downstream of thrombin, in turn; this leads to endothelial

contraction and tension on inter-endothelial junctions, which might rupture in response to this challenge [32,33]. In this manner, Mac^{AIRs} protect the integrity of the tunica intima by seizing PAR-1 cleavage, interrupting thrombin-mediated activation and preventing exposure of the underlying and highly pro-thrombotic matrix. In addition, we found that Mac^{AIRs} identified and phagocytosed endothelial cells undergoing apoptosis (as per expression of annexin) further implying a cell scavenger function of Mac^{AIRs} to promote vascular health.

Supporting the biological role attributed to these macrophages, it is pertinent to remember that while compatible with development and reproduction, plasminogen deficiency results in a severe thrombotic phenotype in both normal and inflamed tissues of adult animals[39,49,50]. Homozygous plasminogen deficient mice display spontaneous thrombotic lesions in multiple organs and a median survival of 176 days with about 40% of the mice succumbing to death. Additionally, these death phenotypes are effectively reversed by the simultaneous imposition of fibrinogen deficiency[39]. These findings underlie a critical constitutive function of the plasminogen activation system for fibrin surveillance and clearance in non-pathological settings and resonate extremely well with the findings described here.

Given the association of Mac^{AIRs} with areas of disturbed flow, also known to be pro-atherogenic sites, their potential contribution to atherosclerotic lesions is an important question. Specifically, one could predict that Mac^{AIRs} are particularly poised to be the progenitors of foam cells. This question was the focus of an elegant study recently published[15]. The authors found that while Mac^{AIRs} can uptake lipids, elimination of these cells only delays slightly, but does not alter the burden of atherosclerotic lesions, nor does it change the accumulation of foam cells in the lesions. Altogether, the conclusions of that study indicate that while participating in the process, it is the influx of circulating monocytes into the neointima that is the main source of foam cells. In context, these data together with the fact that Mac^{AIRs} embed the tunica intima immediately post-birth, are in agreement with the notion that the presence of these macrophages is not a response to a pathological insult.

The present report adjoints to the long list of studies that have recently identified self-renewing tissue-resident macrophages in multiple organs[21,22,28,51-54], now adding the aortic endothelium to this list. These tissue-resident macrophages were found to seed multiple organs either during embryonic development or shortly thereafter, and are derived from either yolk sac erythroid-myeloid or circulating myeloid progenitors[27,28]. Tissue-resident macrophages from distinct organs are found to have unique transcriptional identities and functions and are programmed by an organ-specific niche. As discussed, we attribute endothelial cells conditioned by disturbed flow the niche for Mac^{AIRs} differentiation. Importantly the well accepted pro-inflammatory profile initially unique to the endothelium in areas of disturbed flow is also acquired by aging endothelium. By comparing Mac^{AIRs} from different anatomical regions of aortae in young vs old mice and showing that these macrophages are transcriptionally identical, our results provide evidence that changes in the endothelial cell niche are responsible for the underlying tissue-specific imprinting of these macrophages. The relevance of the microenvironment in promoting a niche cannot be overstated. For example, Kuffer cells (resident macrophages in the liver) are embryonically derived and self-maintained throughout adulthood. However, if depleted using diphtheria toxin models, bone marrow derived monocytes are capable of yielding monocyte-derived

Kuffer cells that are genetically and functionally comparable to the embryonic-derived cells[42-44]. Along these lines, we find that in the absence of constant pressure to eliminate Mac^{AIRs} using diphtheria toxin, monocytes have the ability to quickly repopulate these same sites and differentiate into Mac^{AIRs}.

The findings presented here shift several paradigms. First, they challenge the concept that associations between endothelium with leukocytes are always transient and triggered by acute inflammatory events. In fact, our results highlight a long-term partnership between endothelial cells and macrophages that is not dependent on immune responses, instead it is triggered by the drastic hemodynamic changes associated with birth. Second, they change the view that a homotypic endothelial layer forms the luminal side of vessels; which now needs to be amended to include macrophages in areas of disturbed flow and aged arteries. Lastly, our findings indicate that intravascular clotting in arteries is constantly antagonized in regions of disturbed flow and “aged” endothelium. While the non-thrombogenic function of vessels was attributed exclusively to the endothelium, the data presented here provides clear evidence that in some regions of the vascular tree this can only be accomplished with aid of macrophages. The relevance of this endothelial-macrophage partnership cannot be overstated as per the devastating intravascular clotting sequelae associated with some conditions including COVID19.

METHODS

Data and Code Availability

All data generated or analyzed during this study are included in the Article and its Supplementary Information. The scRNA-seq data were deposited in the GEO database, accession number GSE161787.

Mice

All animal procedures were approved and performed in accordance with the UCLA and Northwestern University Institutional Animal Care and Use Committee. All other mouse information can be found in the Supplementary Table 9. All mouse strains were maintained on a C57BL/6J background, with the exception of CSF1R-merCremer mice, which was maintained on a mix background (FVB:C57BL/6). Mice were genotyped by Transnetxy. Males and females were used in approximately equal numbers for all experiments with the exception of scRNA-seq experiments. For scRNA-seq experiments, only male C57BL/6 mice were used to minimize sex/strain differences at the transcriptional level for the arch (8wk) and aged descending (78wk) A,B data sets. Unless specified, all adult mice used were 8-10wks of age.

Aorta *en face* harvest

Adult mice were injected intra-peritoneally with 10mg of methacholine to promote smooth muscle cell relaxation to facilitate *en face* imaging. Immediately after injection, adult mice were sacrificed and perfused with 10mLs of 2% paraformaldehyde (PFA) through the left ventricle (for embryos and neonates, 0.5-3mLs of 2% PFA was used). Following perfusion, the aortae were removed and the adventitia carefully dissected under a microscope. Aortae

were opened longitudinally, transferred to a 35mm silicon-coated dish filled with 2% PFA and pinned to lay flat, exposing the endothelium. Fixation proceeded for one additional hour at 4°C followed by washes in phosphate buffered saline (PBS).

Aortic *en face* immunostaining

For immunostaining, tissue was washed 3 times with 1X HBSS and then incubated in blocking/permeabilization buffer (0.3% Triton-X, 0.5% Tween-20, 3% Normal Donkey Serum) for 1hr at room temperature. Primary antibody cocktail was prepared in the blocking/permeabilization buffer and incubated overnight at 4°C (endothelial marker ERG, VE-cadherin, or Pecam1 were always used in conjunction with other markers in order to label the endothelium). The following day aortae were washed three times with 1X HBSS and incubated with secondary antibodies with DAPI for 1hr at room temperature. After final set of washes in 1X HBSS, aortas were mounted on glass slides with prolong gold without DAPI (Thermo,# P36930). For list of antibodies and dilutions used, see Supplementary Table 9. Stained aortae were mounded on glass slides with lumen facing the coverslip. Aortae were imaged using either an LSM880 confocal microscope (ZEISS) or an A1R HD25 confocal microscope (Nikon). Z-stack and tile scan features were used to image the large, wavy surfaces of the aortae. The resulting tiles were then stitched into a single large image (ZEN 2.0 Black software, ZEISS or NIS-Elements, Nikon), which enabled the visualization of the large aortic arch with high resolution. Imaris software (Imaris 9.5.1 and 9.7.0 Bitplane) was used to visualize images in 3D. For list of software used for analysis, see Supplementary Table 9. Additionally, Denoise.AI (Nikon) was employed to remove Poisson shot noise in certain images. Images were acquired using either 20x,63x, or 100x objectives.

In vivo labeling

Mice (C57BL/6) of 8wks of age were injected via tail vein with either rat anti-msCD45 antibody or non-blocking Pecam1 (390)-daylight 650 antibody diluted in sterile PBS to label the lumen facing surfaces of Mac^{AIRs}. Mice were sacrificed 15min (for Pecam) and 30mins (for CD45) after injection and aortae were fixed, harvested, and stained with additional, antibodies. For *in vivo* labeling of CD45: additional mouse anti-mouse CD45-biotin / streptavidin-a647, Donkey anti-rat-a488, and Pecam1 (2H8)-a568. For *in vivo* labeling of Pecam1(390)-injected mice: ERG / Donkey anti-Rb-a568, and rt-CD45 / Donkey anti-Rt-a488 (Supplementary Table 9).

Immunostaining and imaging of sections

Formalin fixed, paraffin embedded specimens from kidneys were sectioned at 4um. Antigen retrieval was performed using 1X citrate buffer and then incubated in blocking/ permeabilization buffer for 1hr at room temperature. Sections were then incubated with primary antibodies (Supplementary Table 9) overnight at 4°C. The following day, samples were incubated with species - specific secondary antibodies for 1 hour at room temperature prior to mounting in Prolong Gold without DAPI. Samples were evaluated using an A1R HD25 confocal microscope (Nikon).

Brightfield imaging of the aortae

E18.5, P1, P3, 1wk, 3wk, and 10wk old aortae were dissected and the adventitia was removed under a dissecting microscope. Aortae were pinned onto a 35mm silicon-coated dish filled with PBS. Aortae were imaged using an ECHO-Revolve (RVL-100-G).

scRNA-seq

Isolation of intima cells was as previously described[20]. In summary, mice were anaesthetized and perfused with 10mLs versene buffer through the left ventricle. The adventitia was removed and aorta dissected and cut open in versene buffer so that it laid like a flat sheet, exposing the endothelium. After versene washes, the aortae were bathed in 1X trypsin and incubated for 2X 5min at 37°C. The endothelium was then gently removed using a microscalpel (EMS#72046-30) and repeat pipetting, now with sc-HBSS (containing 0.04%BSA and 2%FBS to inactivate the trypsin and Actinomycin D at 1ug/ml to block transcription) was applied this helped in removing the cells and obtaining a single cell suspension. The procedures were done under a dissecting microscope. Cells were pelleted and then treated with 1X RBC lysis buffer (eBioscience, #00-4333-57) for 1 minute and then washed twice with 0.04%BSA. Schematics of intimal cell isolation is shown in Figure S2A. To obtain enough cells, 6 (aged descending) or 8 (arch) C57BL/6 mice were used per library.

To isolate adventitia cells into single-cell suspension, mice were anaesthetized and perfused with 10mLs of DMEM. The adventitia was dissected from aortae and dissociated using the Miltenyi adipose tissue dissociation kit (#130-105-808). Following Milteny protocol, the single-cell suspension was additionally treated with 1X RBC lysis buffer (eBioscience, #00-4333-57) and 1U DNase. Final cell suspension was washed multiple times and resuspended in 0.04%BSA. A total of six male C57BL/6 mice (78wk old) were used to generate the library.

scRNA-seq libraries were generated using 10X Genomics Chromium Single Cell 3’ Library & Gel Bead Kit v2. Cells were loaded accordingly following the 10X Genomics protocol with an estimated targeted cell recovery of 5000 cells. Sequencing was performed on Illumina HiSeq4000 (Pair-end, 100 base pairs per read, 8wk arch & aged descending A,B). The digital expression matrix was generated by demultiplexing, barcode processing, and gene unique molecular index counting using the Cellranger count pipeline (version 4.0.0, 10X Genomics). Multiple samples were merged using the Cellranger aggr pipeline. To identify different cell types and find signature genes for each cell type, the R package Seurat (version 3.1.2) was used. Cells that expressed <100 genes or <500 transcripts were filtered out. We ran the DoubletFinder algorithm and set the doublet rate at 2%, as recommended by vendor (10X Genomics). The algorithm predicted only 0.01% of doublets were captured. The doublets in our dataset did not pose as new cell types. Variable genes were selected using the FindVariableGenes function for further analysis. The data were normalized using the NormalizeData function with a scale factor 10,000. The genes were then scaled and centered using the ScaleData function. Principal component analysis (PCA) and *t*-distributed stochastic neighbor embedding (t-SNE) were used to reduce the dimensionality of the data. The cluster marker genes were found using the FindAllMarkers function. Cell types were

annotated based on the cluster marker genes. Heatmaps, violin plots and gene expression plots were generated by DoHeatmap, VlnPlot, FeaturePlot functions, respectively.

Flow Cytometry of peripheral blood

To measure reporter labeling (lineage tracing) and donor chimerism (parabiosis mice) of circulating cells, blood was collected by retro-orbitally bleeding into tubes containing FACS buffer at 4°C. Blood cells were pelleted and treated with 1X RBC lysis buffer. Additionally, cells were stained on ice with CD45-APC-Cy7 (BD, #557659) and then analyzed on a BD Fortessa.

Flow cytometry of organs: One-day post-diphtheria toxin injection (Mac^{AIR}-depletion), littermate control and $Cx3cr1^{creERT2}$;$CSF1R^{lslDTR}$ were euthanized and perfused with 10mL of versene to remove blood and then perfused with 10mLs of DMEM. Lung, liver, kidney, and leg bone (femur and tibia) were carefully dissected and washed in PBS. For bone marrow harvest, muscle was removed and bone was cleaned. Bone was then crushed in FACs Buffer using a motor pestle to release bone marrow cells. Bone marrow cells were then pelleted and treated with 1X RBC lysis buffer. For generation of single-cell suspension from lung, liver, and kidney, tissues were digested using Militenyi's lung dissociation kit (#130-095-927), liver dissociation kit (#130-106-807), and multidissociation kit #2 (#130-110-203), following vendor's protocol. Cells were pelleted and treated with 1X RBC lysis buffer. Additionally, bone marrow, lung, liver, and kidney cells were stained on ice with CD45-APC-Cy7 (BD, #557659), CX3CR1-APC (BioLegend, #149008), CSF1R-BV421 (BioLegend, #135513), and Ter119-PECy7 (eBioscience, #25-5921-82) then analyzed on a BD Fortessa.

Lineage Tracing

Homozygous lox-stop-lox-tdTomato reporter mice were crossed with homozygous Cx3cr1-creERT2 mice. Tamoxifen induction of CRE activity in the resulting F1 compound heterozygotes was initiated by dissolving tamoxifen (Free base, MP Biomedicals, #0215673891) in sunflower seed oil (Sigma #S5007) and administering 0.01mg of tamoxifen via oral gavage to neonates at P1, P3, and P5. The penetration of intimal tdTomato positive CD45 positive cells in the aorta at P7 ranged from 40-62% determined by *en face* confocal imaging (Fig. 3f), thus the analysis in the 4wk adult needed to be normalized to P7 littermates. Therefore, as a baseline control, half of the litter was sacrificed and blood, as well, as the aorta were collected to determine reporter labeling efficiency. At 4wks, the remaining littermates were sacrificed and blood as well as aorta were collected to determine reporter expression.

To induce reporter expression in adult Cx3cr1-creERT2; R26-lox-stop-lox-tdTomato were administered 1mg of tamoxifen intra-peritoneal (IP) three times, every other day. The penetration of tdTomato positive intimal CD45+ cells in the aorta ranged from 97-100%. Aortae and blood were collected at 1wk-post as a baseline control for normalization purposes. The rest of the littermates were sacrificed 10-weeks post-injection to access retention of reporter expression in adulthood.

For clonal tracing, Cx3cr1-creERT2; R26-Rainbow neonates were administered 0.01mg of tamoxifen via oral gavage at P1, P3, and P5 to yield permanent expression of three mutually exclusive fluorescent protein labels: Cerulean, mOrange, and mCherry. At 8wks, mice were sacrificed and reporter labeling was assessed. Adult Cx3cr1-creERT2; R26-Rainbow were injected with one dose of 0.02mg of tamoxifen and aortae were assessed 9 months later.

In vivo macrophage depletion

To deplete macrophages, adult (8-10w) Cx3cr1-creERT2;CSF1R-flox-stop-flox-DTR mice, were first injected with tamoxifen IP to promote Cre-dependent induction of the diphtheria toxin receptor (DTR). The following day, mice were injected with 200ng of diphtheria toxin (Sigma, #D0564) in sterile 1X PBS to induce apoptosis of DTR-expressing cells. This resulted in cell death of this population as quickly as 24hrs. However, since intimal, aortic myeloid cells are replenished quickly, evaluation of longer time-points required continuous injection with tamoxifen followed by diphtheria toxin every three days until the end of the experiment.

EdU incorporation assay

Mice were injected IP with EdU (5-ethynyl-2-deoxyuridine, Fisher Scientific, #A10044 at 10mM). Two hours post-injection, mice were terminally anesthetized and perfused with 2%PFA via the left ventricle. The aorta was removed and the adventitia dissected away. The aorta was longitudinally cut and pinned so that the endothelium was exposed. Following fixation, EdU was revealed using a647 following manufacture's protocol (Invitrogen #C10640). Additionally, aortae were stained for nuclear endothelial marker ERG, pan-hematopoietic marker CD45, and DAPI before being imaged (Supplementary Table 9).

Scanning Election Microscopy

To determine the location of macrophages in relation to the endothelium, mice were anesthetized and perfused with 10mLs of 2% PFA through the left ventricle. Aortae were first immunostained *en face* following the protocol listed above. High- and low-resolution images were then obtained by confocal microscopy. After imaging, the aortae were washed in 1X HBSS, dehydrated with increasing concentrations of ethanol, and subjected to critical point drying followed by gold/palladium coating using a sputter coater. High- and low-resolution SEM images were also taken in order to utilize landmarks and find macrophages identified with the confocal images. Confocal images and SEM images were then overlaid together using Adobe Photoshop.

To image microclots in macrophage-depleted ($Cx3cr1^{creERT2}$;$CSF1R^{lslDTR}$) and control aortae, mice were perfused with 4% Glutaraldehyde through the left ventricle. Aortae were dissected and treated for an additional 1hr in 4% Glutaraldehyde at room temperature and then washed several times with 1X PBS. Aortae were then incubated in 1% osmium tetroxide for 1hr, dehydrated in a series of ethanol, dried in critical point mounted on pins, and coated with 10nm gold for SEM. Aortae were then imaged using JEOL NeoScope at 10kV or15kV.

Dabigatran treatment

Mice were injected 2X a day (morning and night) intraperitoneal with 300ug of Dabigatran (BIBR 953, Selleck #S2196) per injection for 5 days. Dosage was determined by clotting test. After 5-days of treatment, mice were sacrificed and aortae were analyzed.

In vivo siFibrinogen knock-down

8wk C57BL/6 mice were weighed and then injected with either siFibrinogen or siRNA targeting Luciferase (siLuciferase, control) at 1mg siRNA per kg body weight via tail vein injection. siFibrinogen and siLuciferase were each encapsulated in lipid nanoparticles, composed of an ionizable lipid (DLin-MC3-DMA), phosphatidylcholine, cholesterol, and a poly-ethylene glycol lipid, using methods previously described [55]. To determine knock-down efficiency, we quantified fibrinogen protein levels in plasma 7-days post-injection. In short, we collected peripheral blood in EDTA-coated tubes (BD #365974) and isolated plasma via centrifugation. Plasma was diluted (1:50) and fibrinogen was measured using a Mouse Fibrinogen ELISA kit (Abcam #ab213478).

Intravenous administration of Fibrinogen-a488 or Plasminogen-FITC

Mice were injected intravenously with 400ug of Fibrinogen-a488 (Thermo #F13191), plasminogen-FITC (Abcam #ab92770), or Albumin-FITC (control, Thermo #A23015). Fibrinogen-a488 injected mice were sacrificed 3-hrs post-injection and plasminogen-FITC injected mice were harvested 4-hrs post-injection to assess local accumulation, relative to the Mac^{AIRs}.

D-dimer measurements

Mice were anesthetized and blood was collected via right ventricle puncture with a 25G syringe. For D-dimer measurements, blood was collected in citrate buffer with a final ration of 3.2% citrate (for D-dimer). Blood was centrifuged and citrate plasma was collected and shipped to IDEXX on dry ice for quantification.

Comparison to the Tabula muris atlas and Chakarov et al. 2019

To find similar cell population in other tissues, we compared the MacAIRs to the monocytes/macrophages from the Tabula Muris Atlas. Specifically, the expression values for all the monocytes and macrophages were extracted from the Tabula Muris Atlas and merged with the expression values of the MacAIRs from our dataset. The Seurat pipeline described above was applied to cluster the cells. Since the datasets were generated by different labs, the RunHarmony function from the R package harmony[56] was applied to remove potential batch effects among different tissues. After clustering, the MacAIR marker genes were used to calculate a module score, which was used to identify the cell population from the Tabula Muris Atlas that were similar to the MacAIRs. The module score was calculated based on the average expression of the genes in the list, subtracted by the aggregated expression of randomly chosen control genes.

Monocytes and macrophages obtained in our scRNAseq datasets were also overlapped to the two macrophage populations obtained by Chakarov *et al.* [22]. For this marker genes extracted

from the comparison among the monocytes, adventitia macrophages and MacAIRs in our study were compared to the Lyve1^{lo}MHCII^{hi} and Lyve1^{hi}MHCII^{lo} from the Chakarov study. The Jaccard index between each pair for cell types from the two datasets was calculated and plotted in the heatmap.

Parabiosis

Mice of the similar weight, size, and same sex were housed together for 2 weeks prior to surgery to assess compatibility. Surgeries were done as previously [57]. In short, mice were anesthetized and matching skin incisions were made from the olecranon to the knee joint of each mouse, and the subcutaneous fascia was bluntly dissected to create ≈0.5 cm of free skin. The right olecranon of 1 animal was attached to the left olecranon of the other by a single 3-0 nylon suture and tie. The partners' knee joints were similarly connected. The dorsal and ventral skins were closed approximated by staples, and the animals were warmed with heating pads and monitored until recovery. Parabiotic pairs were housed 1 pair per cage and given acidified water (pH 2.5). After 4 weeks of anastomosis, blood samples from each animal in a parabiont pair were analyzed using flow cytometry. Animal pairs with <30% blood chimerism were excluded from our studies.

Annexin staining in aortae

Adult mice were sacrificed and perfused with 3mLs of 5% Annexin-a488 conjugate (Invitrogen, #A13201) through the left ventricle. After a couple of minutes, the aorta was carefully dissected and transferred to a 35mm silicon-coated dish filled with 20% Annexin-a488. 20% Annexin-a488 was also used to flush the Annexin inside the intact vessel and then incubated at 37°C for 10min. Following incubation, the tissue was fixed in 2%PFA for one additional hour at room temperature followed by multiple washes on PBS. The aortae were then opened and pinned to lay flat, exposing the endothelium and immunostained as described previously with ERG, CD45, and DAPI (Supplementary Table 9).

In vitro thrombin and MMP13 treatment and thrombin treatment with shear stress

Human aortic endothelial cells (HAECs) were isolated as described from aortic trimmings of donor hearts at the University of California, Los Angeles (UCLA) [58]. All HAECs were de-identified and exempt from consideration as human subjects research by institutional regulatory boards at UCLA. Additional HAECs were purchased from Lonza (#CC-2535). For thrombin and MMP13 treatment, HAECs were grown on gelatin-coated, tissue culture-treated six-well plates (Falcon, #353046) to confluency in complete MCDB-131 media (VEC Technologies #MCDB131-WOFBS) plus 10% FBS (Omega-Scientific#FB-11). Once confluent, cells were washed with PBS to remove serum, then serum-free MCDB-131 was added to HAECs for overnight starvation. Next day, cells treated with Vehicle, MMP13 (1ug, Abcam #ab227435), or Thrombin (0.625U/mL, Sigma #10602400001) for 5 mins. After treatment, cells were washed in PBS with Na3OV4 and lysates were collected using mRIPA (50mM Tris, 0.1%SDS, 0.5% Na-Deoxycholate, 1%Triton-X, 150mM NaCl, 1mM Na3VO4, Protein inhibitor cocktail). Lysates were denatured in Laemmli buffer with 2-Mercaptoethanol at 95°C for 10 minutes. Proteins were separated by SDS-PAGE gradient (4-20%, Bio-Rad #4561094DC) gel and transferred onto nitrocellulose membranes (Bio-rad #1704271) and incubated overnight at 4°C with primary antibodies. Primary

antibodies: anti-phosphorylated MLC2 (3671S), anti-MLC2 (CST #3672S), Par1 (Thermo #PA5-19102), gamma-tubulin (Abcam #ab11321). HRP-conjugated secondary antibodies (1:10,000) were applied in species dependent manner for 1hr at room temperature. Immuno-complex detection was enhanced chemiluminescence SuperSignal™ West Femto Maximum Sensitivity Substrate (ThermoFisher Scientific #34095) using ChemiDoc XRS + Molecular Imager (Bio-Rad Laboratories). Quantification of bands was performed using ImageLab Software (Bio-Rad Laboratories).

For thrombin and shear stress experiments, HAECs were grown on gelatin-coated, glass-bottom, six-well plates (Cellvis, #P06-1.5H-N) to confluency in complete MCDB-131 media plus 10% FBS. Once confluent, cells were washed with PBS to remove serum, then media containing MCDB-131 and 4% dextran (Sigma-Aldrich #31392) was added to confluent HAECs. Vehicle (PBS) or thrombin (Sigma, #10602400001) to a final concentration of 0.625 U/mL was then applied. Monolayers were subjected to unidirectional constant laminar flow for 48hrs at 130rmp horizontal circular orbit (Benchmark, #BT302). Static monolayers used the same dextran-containing media and were cultured alongside flow-treated monolayers. 48hrs-post flow, cells were fixed in 2%PFA for 15 minutes at room temperature, then washed in PBS.

For immunostaining, cells were incubated in blocking/permeabilization buffer (0.3% Triton-X, 0.5% Tween-20, 3% Normal Donkey Serum) for 1hr at room temperature. Primary antibody cocktail was prepared in the blocking/permeabilization buffer and incubated overnight at 4°C. The following day aortae were washed three times with 1X PBS and incubated with secondary antibodies for 1hr at room temperature. All primary cells were cultured in humidified incubator at 37°C and 5% CO_2 and used between passages 4 and 9.

Microspheres permeability

One-day post-diphtheria toxin injection (Mac^{AIR}-depletion), littermate control and $Cx3cr1^{creERT2}$;$CSF1R^{lslDTR}$ mice were injected in the left ventricle with 200uL of 40nm microspheres (1:10, Thermo #F8795). Beads circulated for 5 mins and then mouse was euthanized and perfused with 10mLs of PBS followed by 10mLs of 2%PFA. Aorta harvest and whole-mount staining was performed as described above. For positive control, C57BL/6 mice were injected with 50mM EDTA buffer solution in the left ventricle and allow to circulate for 5mins to challenge endothelial junctions. Then, these positive control mice were injected with microspheres and harvested as described.

Tail Bleeds

One-day post-diphtheria toxin injection (Mac^{AIR}-depletion), littermate control and $Cx3cr1^{creERT2}$;$CSF1R^{lslDTR}$ mice with same age/weight were anesthetize with ketamine/xylazine at a dose of 0.1mL/20g. Using scalpel blade #11, mice's tails were resected exactly 3mm of distal tail. Tails were quickly placed in tail bleeding buffer (10mM Tris-HCL, 2mM CaCl2, warmed to 37C), starting stopwatch. Stopwatch was stopped after blood stream halted.

Ex vivo Nitric Oxide (NO) measurements

5mM stock solution of DAF-FM diacetate (Invitrogen, #D3844) was diluted to 10uM in media without phenol red (EBM, Lonza#CC-3129). One-day post-diphtheria toxin injection (Mac^{AIR}-depletion), littermate control and $Cx3cr1^{creERT2}$;$CSF1R^{lslDTR}$ mice were euthanized and perfused with 10mL of PBS followed by 3mLs of 10uM of DAF-FM diacetate. Aortae were then quickly and gently harvested in 10uM of DAF-FM. Intact aortae were then incubated in DAF-FM for 10mins at 37°C. After 10mins, DAF-FM was replaced with fresh DAF-FM and incubated for an additional 15mins. Aortae were then quickly filet open and mounted with PBS. Confocal imaging occurred immediately after to measure NO production.

Quantification and statistical analysis

Treatments were randomized; investigators were blinded to allocation for outcome assessment. Quantification of intimal immune cells in aortae was done using the spots function in Imaris 9.5.1 or 9.7.0 (Bitplane) on maximum intensity Z-projections. Only cells with clearly distinguishable bodies and nuclei (DAPI, not shown) were quantified.

Cell surface area and elongation factor of endothelial cells in control and macrophage-depleted ($Cx3cr1^{creERT2}$;$CSF1R^{lslDTR}$) aortae was determined in several regions of 44.1 mm^2 within the lesser curvature of each whole-mount, flat-mounted aortae. Measurements were done in NIS-Elements, using a combination of manual and automated cell shape identification. VE-cadherin or Pecam1 staining was used to define endothelial cell borders. Experiment included littermate controls that received both tamoxifen and DTx injections. Mean fluoresce intensity (MFI) was determined using the surface function in Imaris 9.5.1 or 9.7.0 on maximum intensity Z-projections. Subsequently, the mean for at least three independent samples and standard deviation of the determined. To assess whether two datasets were significantly different, we calculated P values with unpaired, non-parametric student's *t*-test followed by Mann-Whitney test; $P < 0.05$ was considered significant and $P < 0.05$, 0.01, 0.001 and 0.0001 were represented by *,**,***, and ****. Statistical analyses were performed with Prism 8 (GraphPad Software).

Extended Data

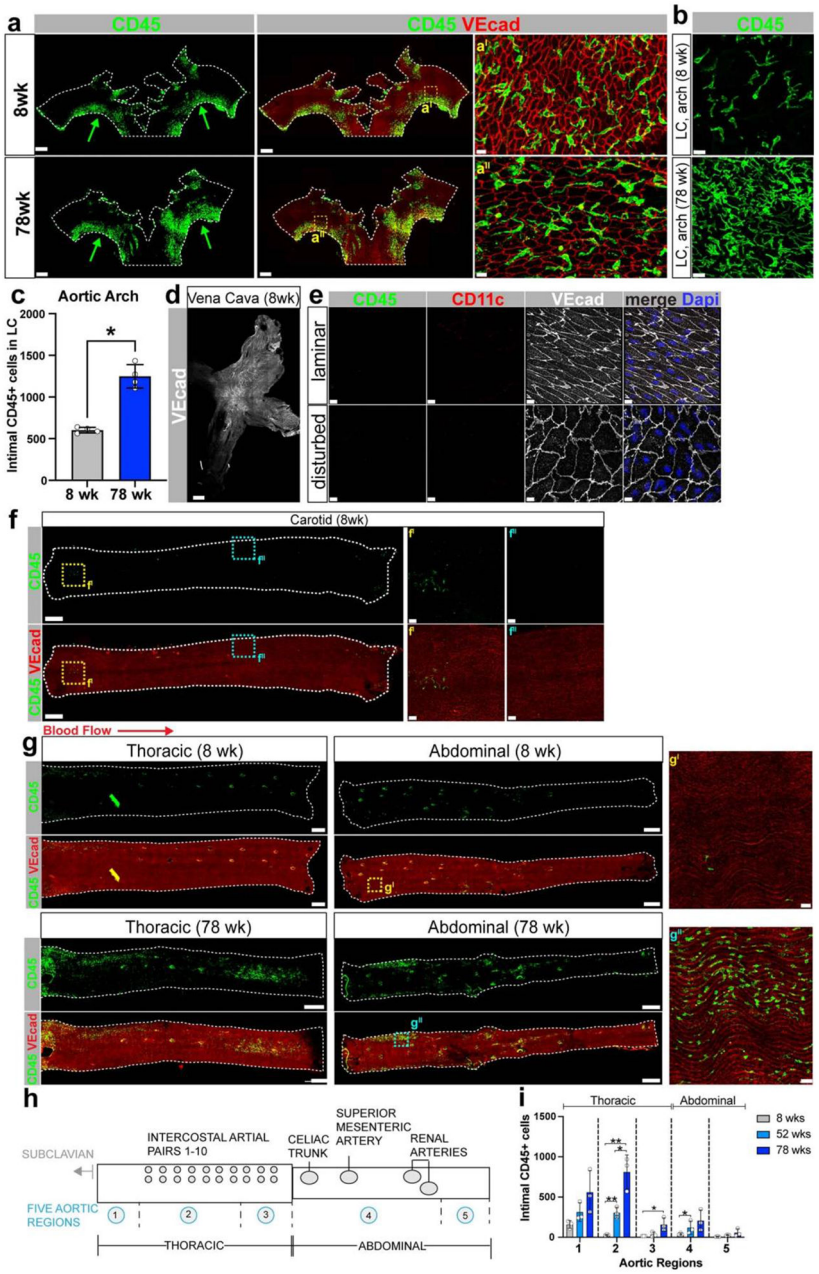

Extended Data Fig. 1: Intimal immune cell distribution in the aorta and vena cava of young and aged mice.

a, Accumulation of intimal immune cells, as per CD45 (green arrows) in adult (n = 498 mice) and old 78wk (n = 6 mice) aortic arch. VE-Cadherin (red). Scale bars, 500μm & 15μm (a^{I-II}). **b**, High magnification of *en face* distribution of CD45 + (green) cells in the lesser curvature (LC) of adult and aged aortae. Scale bar, 20μm. **c**, Quantification of intimal CD45 + cells in LC of 8wk and 78wk old mice. (n = 4 mice per group, Mann-Whitney *T*-test, ± SD, p = 0.0286, two-tailed, *p ≤ 0.05). **d, e** Images of the vena cava of 8wk old mice. **d**, Low magnification of vena cava (VE-Cadherin in white). Scale bar, 500μm. **e**, No

intimal CD11c + (red) CD45 + (green) cells were found in the vena cava, even in regions of disturbed blood flow (Scale bar, 10μm, n = 3 mice). **f**, Few intimal CD45 + cells (green) accumulate in carotid arteries (8wk), VE-Cadherin in red (Scale bar, 300μm, 50μm (f^{I-II}), n = 8 mice). High magnification inserts on the right showing carotid branches (disturbed flow). **g**, Whole mount scans of the descending aortae (thoracic and abdominal) of 8wk and 78wk old C57BL/6 mice. Except for branches, few intimal CD45 + cells (green) were detected in 8wk old descending aortae, (g^{I}) whereas 78wk old mice display large number of intimal CD45 + cells (g^{II}). Scale bar, 500μm (8wk thoracic), 700μm (8wk abdominal), 1000μm (78 wk thoracic and abdominal), and 50μm (g^{I-II}), n = 5 (8wk) and 6 (78wk) mice. **h**, Topographic map to guide the quantification of immune cells shown in '**i**'. **i**, Intimal CD45 + cells per aortic region at 8wk, 52wk, and 78wk old mice (n = 3 mice per timepoint, two-tailed *T*-test, ± SD, p = 0.0022 (2: 8wk vs 52wk), p = 0.0031 (2: 8wk vs 78wk), p = 0.0175 (2: 52wk vs 78wk), p = 0.0396 (3: 8wk vs 78wk), p = 0.0052 (5: 8wk vs 52wk), (*p ≤ 0.05, **p ≤ 0.01).

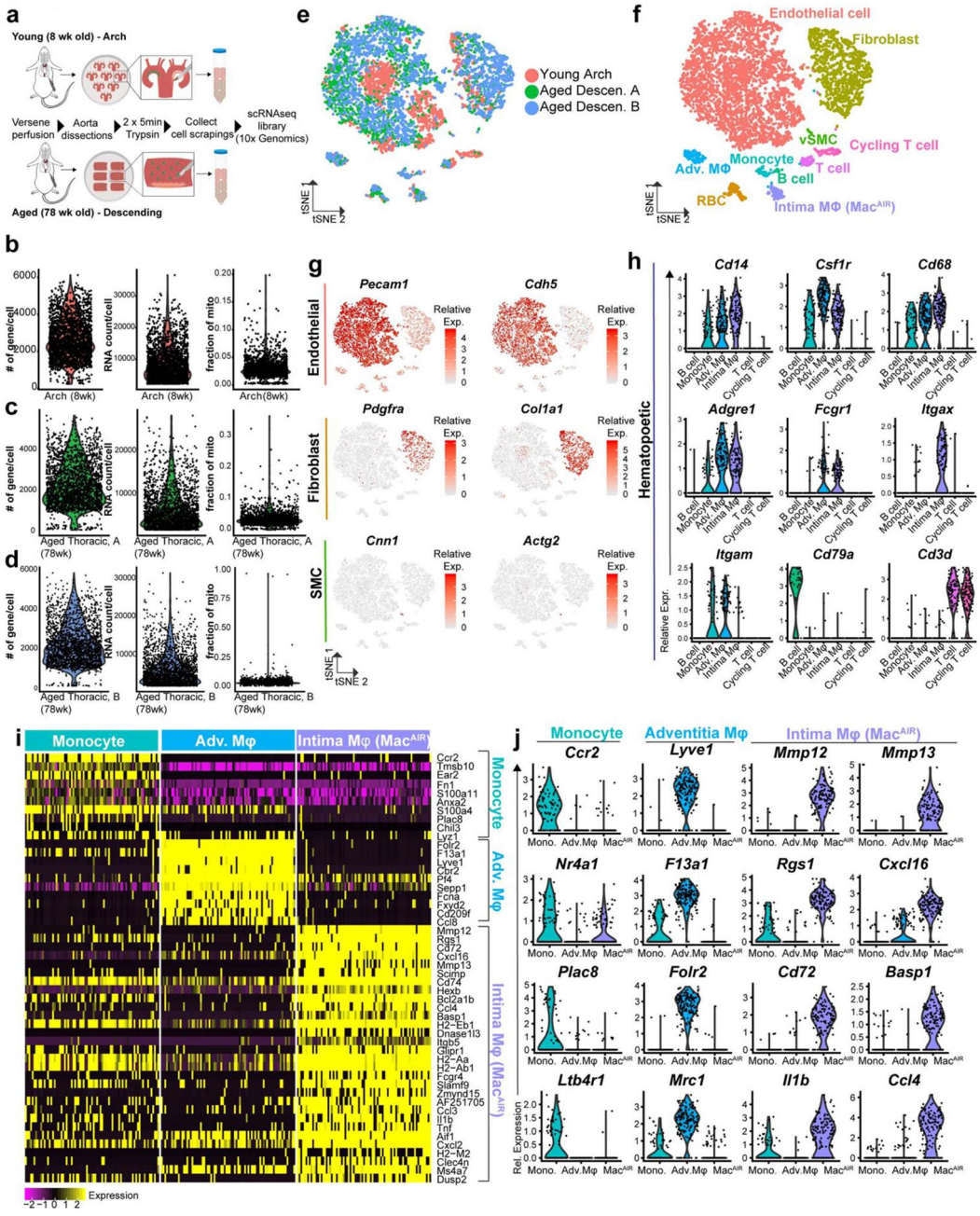

Extended Data Fig. 2: scRNA-seq uncovers the macrophage identity and unique transcriptional signature of the intimal immune cell population.

a, Schematic to illustrate the process for isolation of intimal, aortic cells for single-cell RNA sequencing. **b-d**, Violin plots representing the Quality Control (QC) metrics for each scRNAseq library: Arch and Aged Thoracic A and B. Note, Aged Thoracic A & B represent two independent libraries, not technical replicates, each composed of cells isolated from 6-8 aortae. Shown are: the number of genes per cell (nGene), the absolute number of observed transcripts per cell (nUMI, Unique Molecular Identifier), and the fraction of transcripts arising from the mitochondria genome (fration of mito). **b**, Aortic arch library (red); **c**, Aged thoracic library A (green); **d**, Aged thoracic library B (blue). **e**, tSNE plot

of cells from three independent libraries: aortic arch in red (8 wk) and aged descending (descen.) A (in green) and B (in red) (78wk). 6-8 aortas were used per library. **f**, Ten distinct cell types were identified, and cellular identities were assigned to each cluster. **g**, tSNE analysis and heat map-style representation of non-hematopoietic vascular lineage markers (color key indicates expression level). **h**, Violin plots showing expression levels of the most prominent hematopoietic lineage markers shown as normalized gene expression per cell**. i**, Top differentially expressed genes expressed by monocytes, adventitia macrophages (Adv. Mϕ), aortic intima-resident macrophages (Mac^{AIR}) (color key indicates expression level). **j**, Violin plots showing expression levels of selected genes that distinguished monocytes (left column), Adv. Mϕ (center left column), and Mac^{AIR} (right columns).

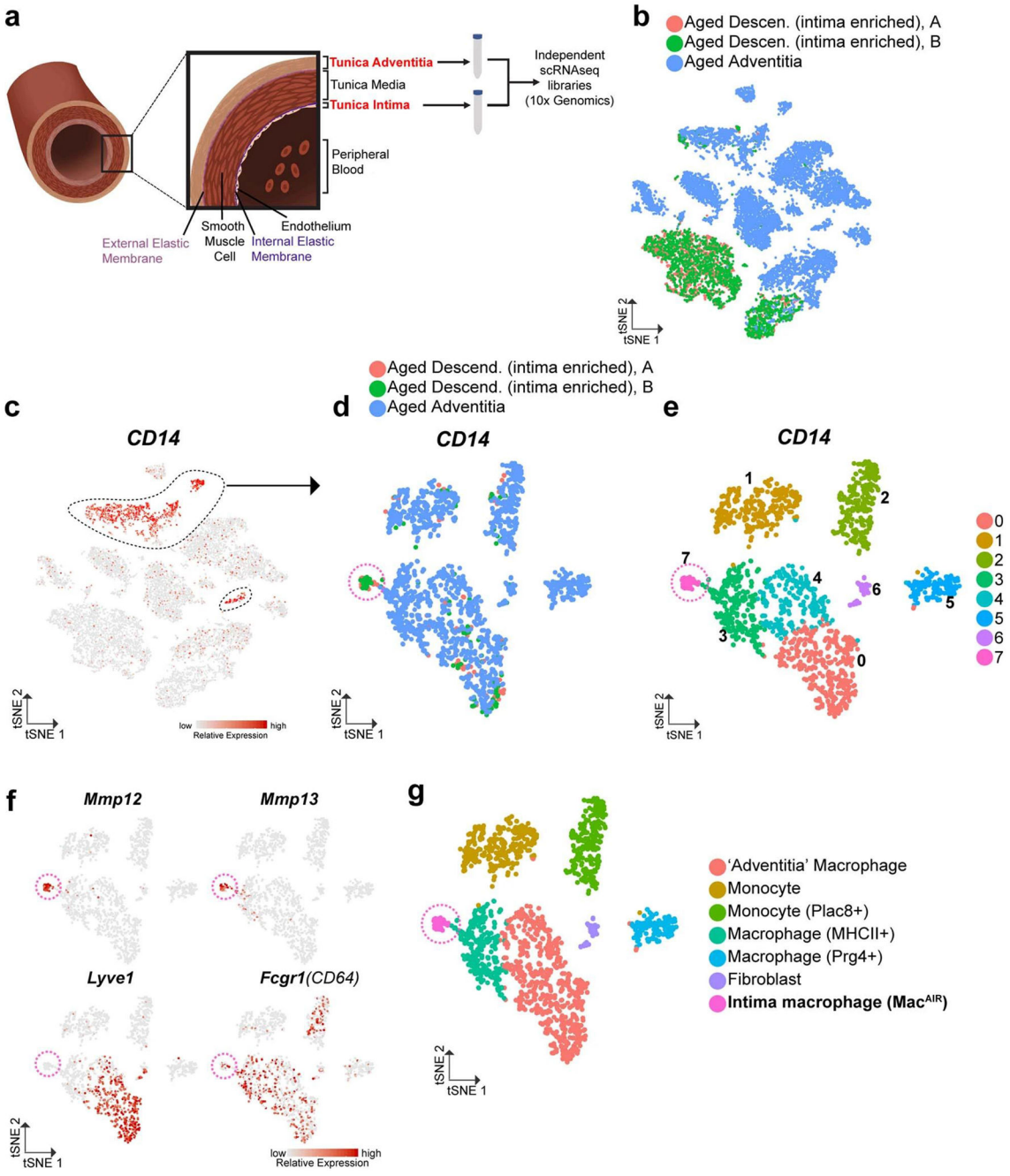

Extended Data Fig. 3: scRNAseq on dissected adventitia.

a, Illustration displaying the different aortic layers and highlighting the tissue that was dissected and used to generate independent scRNAseq libraries for comparison: tunica adventitia vs tunica intima, (red text). b, tSNE projections of cells from three independent libraries: aged adventitia (78 wk) and aged thoracic A and B (78wk). c, Expression of *CD14* to identify myeloid cells in aged thoracic and aged adventitia data sets (color key indicates expression level). d, tSNE plot displaying only the *CD14* expressing cells from c. Pink dotted circle highlights a cluster of cells that are exclusively found in intimal-enriched libraries (Aged Thoracic A and B). e, tSNE plot identifying unique cell clusters presented in

d. Note, cluster 7 (pink dotted cluster) is a clearly distinct population. f, Expression of *Lyve1* was used to identify adventitia macrophages and *Fcgr1* was used to identify macrophages. Note, Cluster 7 expresses *Fcgr1* and also highly expresses *Mmp12* and *Mmp13* but it does not express *Lyve1* (color key indicates expression level). g, Cellular identities assigned to each cluster identified based on transcriptional expression patterns.

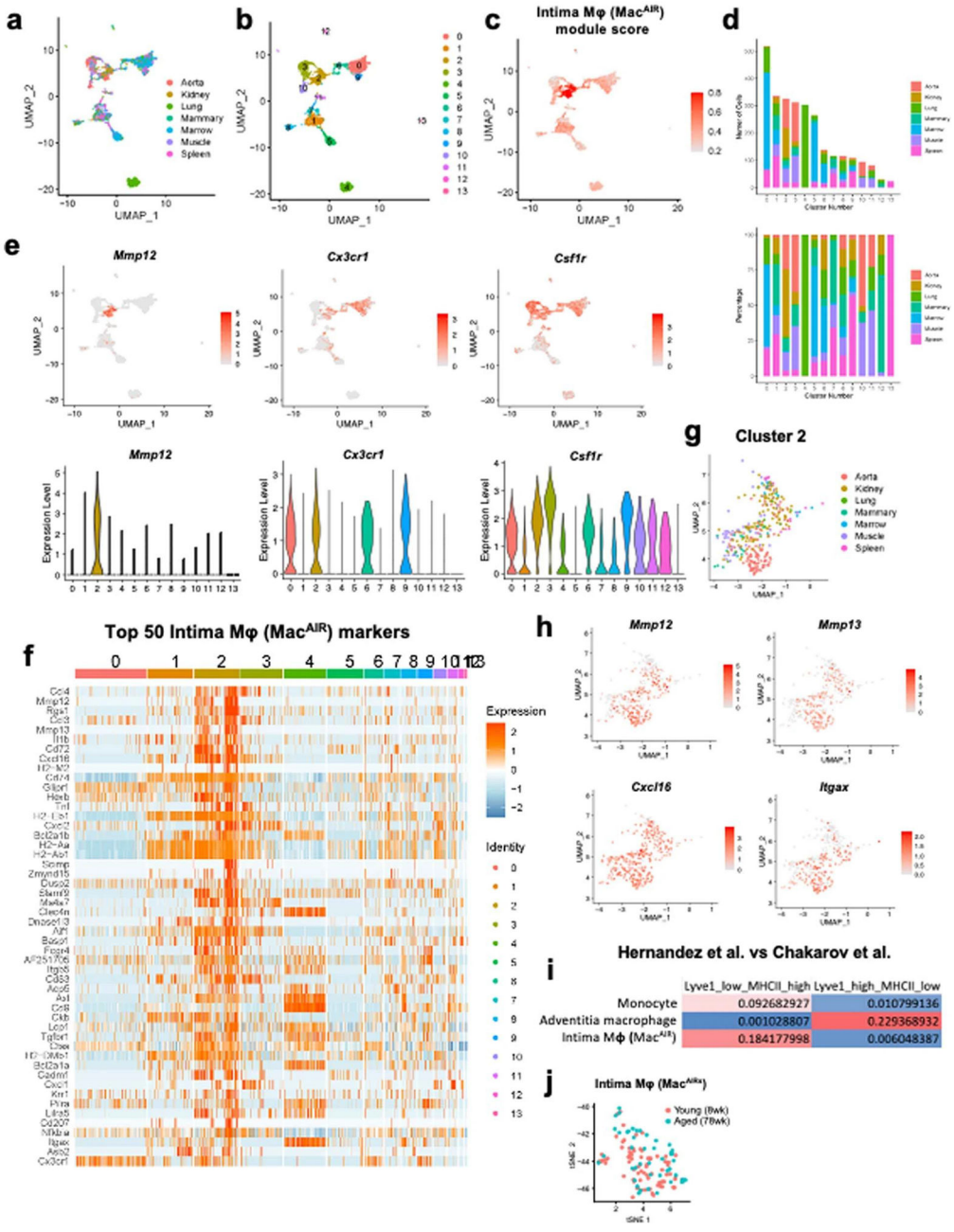

Extended Data Fig. 4: Mac^{AIR} comparison to other published macrophage data sets.
a, Uniform manifold approximation and projection (UMAP) plot of monocytes and macrophages extracted from the Tabula muris atlas and merged with the aortic intima-macrophage (Mac^{AIR}) data set ('Aorta') from this work. **b**, UMAP plot identifying distinct

cell clusters based on transcriptional signatures. **c**, Mac^{AIR} marker genes were used to calculate a module score, which was used to identify cells from the Tabula muris atlas that were similar to Mac^{AIR}. The Mac^{AIR} module score was applied and represented by heat map-style UMAP plot. **d**, Number (top graph) and percentage (bottom graph) of cells from each tissue that are in each cluster. **e**, UMAP heat map-style representation of MMP12 (Mac^{AIR} marker), Cx3cr1, and Csf1r (top row) with violin plot representation of each given gene below. **f**, Heat map comparing the top 50 MacAIR markers to all the clusters found in b. **g**, UMAP plotting only cluster 2 and showing tissue origin. **h**, UMAP heat map-style representation of top Mac^{AIR} markers: Mmp12, Mmp13, Cxcl16, Itgax (CD11c), **i**, Differential genes from the comparison among monocytes, adventitia macrophages, and Mac^{AIR} (our data – this study) were overlapped with genes extracted from the comparison between the $Lyve^{low}MHCII^{high}$ and $Lyve^{high}MHCII^{low}$ macrophages from the Chakarov et al. dataset. The jaccard index between each pair for cell types from the two datasets were calculated and plotted in the heatmap. **j**, Comparison of Mac^{AIRs} identified in the tunica intima-enriched young arch vs aged descending data sets.

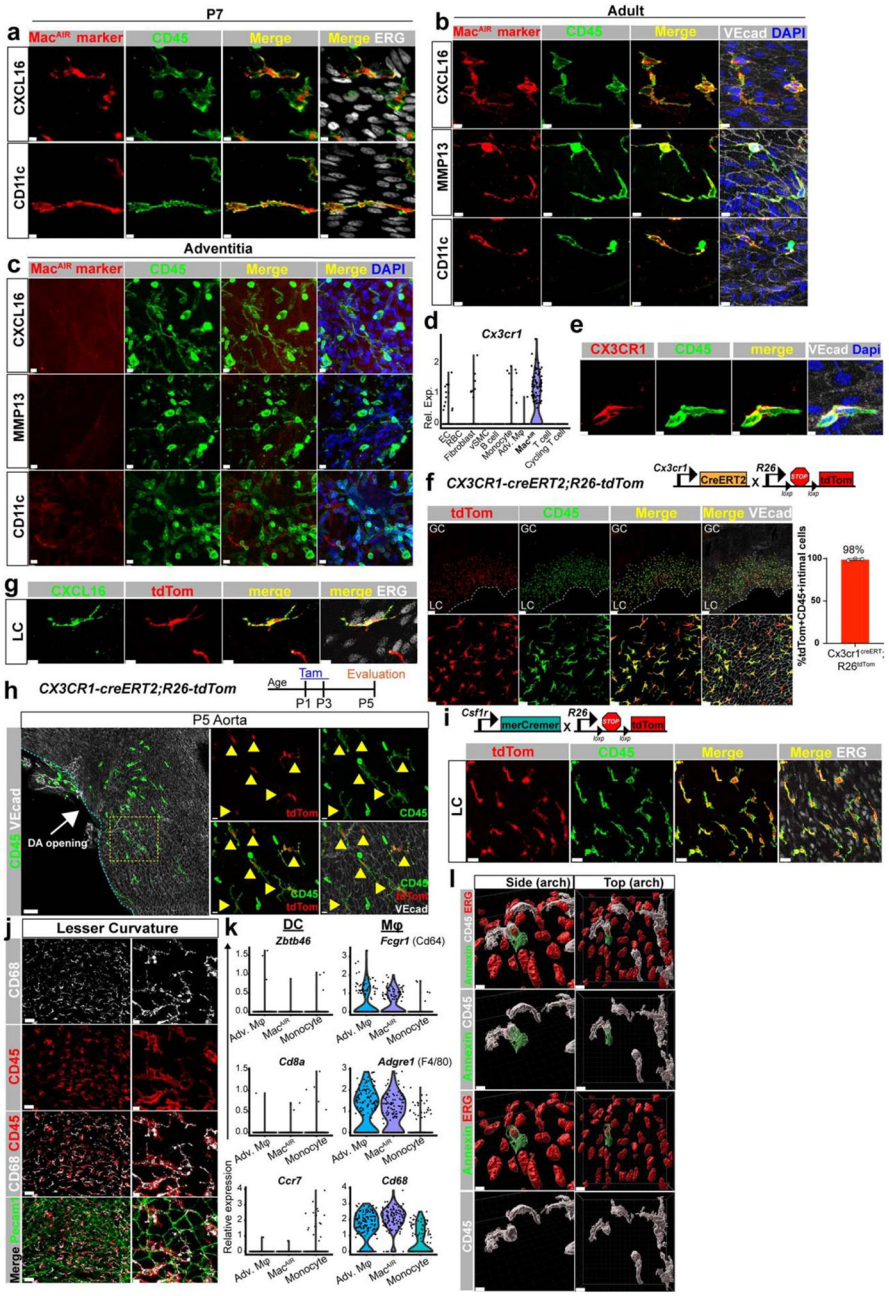

Extended Data Fig. 5: Validation of Mac^{AIR} markers identified by scRNAseq.

a, b, Validation of unique Mac^{AIR} genes at P7 (a) and adult (b) aortae. Mac^{AIR} markers in red (CXCL16 MMP13 and CD11c) and CD45 in green. Scale bar, 5μm and 10μm, n = 3 (P7), 5 (adult) mice. **c**, Evaluation of the same markers as in panels a and **b**, but now in the adventitia. Note that no CD45 + cells in adult adventitia expressed the Mac^{AIR} markers CXCL16, MMP13, and CD11c. Scale bar, 10μm; n = 3 mice per marker. **d-e**, Mac^{AIRs} express Cx3cr1 at both the (**d**) transcript level and (**e**) protein level (in red) (Scale bar, 5μm, n = 3 mice). **f**, Cx3cr1-reporter (Cx3cr1^{creERT2};R26^{tdTomato}) showing tdTomato reporter expression in intimal immune cells one-day post-tamoxifen (Scale bar, 100μm and 30μm). 98% of intimal CD45 + cells in the lesser curvature (LC) of adult

Cx3cr1^{creERT2};R26^{tdTomato} mice were tdTomato + ; represented on adjacent graph (n = 3 mice, ± SD, GC, greater curvature). **g**, Intimal tdTomato+ cells colocalize with Mac^{AIR} marker Cxcl16, post-tamoxifen injection in Cx3cr1^{creERT2};R26^{tdTomato} aortae. Scale bar, 10μm, n = 3 mice. **h**, CD45 + cells found in P5 Cx3cr1^{creERT2};R26^{tdTomato} aortae were also tdTomato + (yellow arrowheads) after tamoxifen at P1 and P3 (Scale bar, 50μm and 10μm, n = 3 mice). VE-Cadherin (white). (DA, Ductus arteriosus). **i**, Csf1r^{merCremer};R26^{tdTomato} macrophage fate-mapping. Intimal CD45 + cells in the lesser curvature (LC) labeled by tdTomato. Adult mice received a single injection of tamoxifen. ERG (white) (Scale bar, 20μm; n = 2 mice). **j**, Images co-staining for CD68 (white), CD45 (red) and VE-Cadherin (green). Scale bar, 30μm and 7μm, n = 3 mice. **k**, Expression of classical dendritic cell (DC) markers (*Zbtb46*, *Cd8a*, *Ccr7*) and macrophage (Mϕ) markers (*Fcgr1*, *Adgre1*, *Cd68*) in adventitia macrophages (Adv. Mϕ), intima-resident macrophages (Mac^{AIRs}), and monocytes from scRNA-seq data in Extended Data Fig. 2. **l**, 3D surface rendering of an intimal CD45 + cell (white) phagocytosing an annexin + (green) endothelial cell (ERG +, red) in the LC. Scale bar, 10μm.

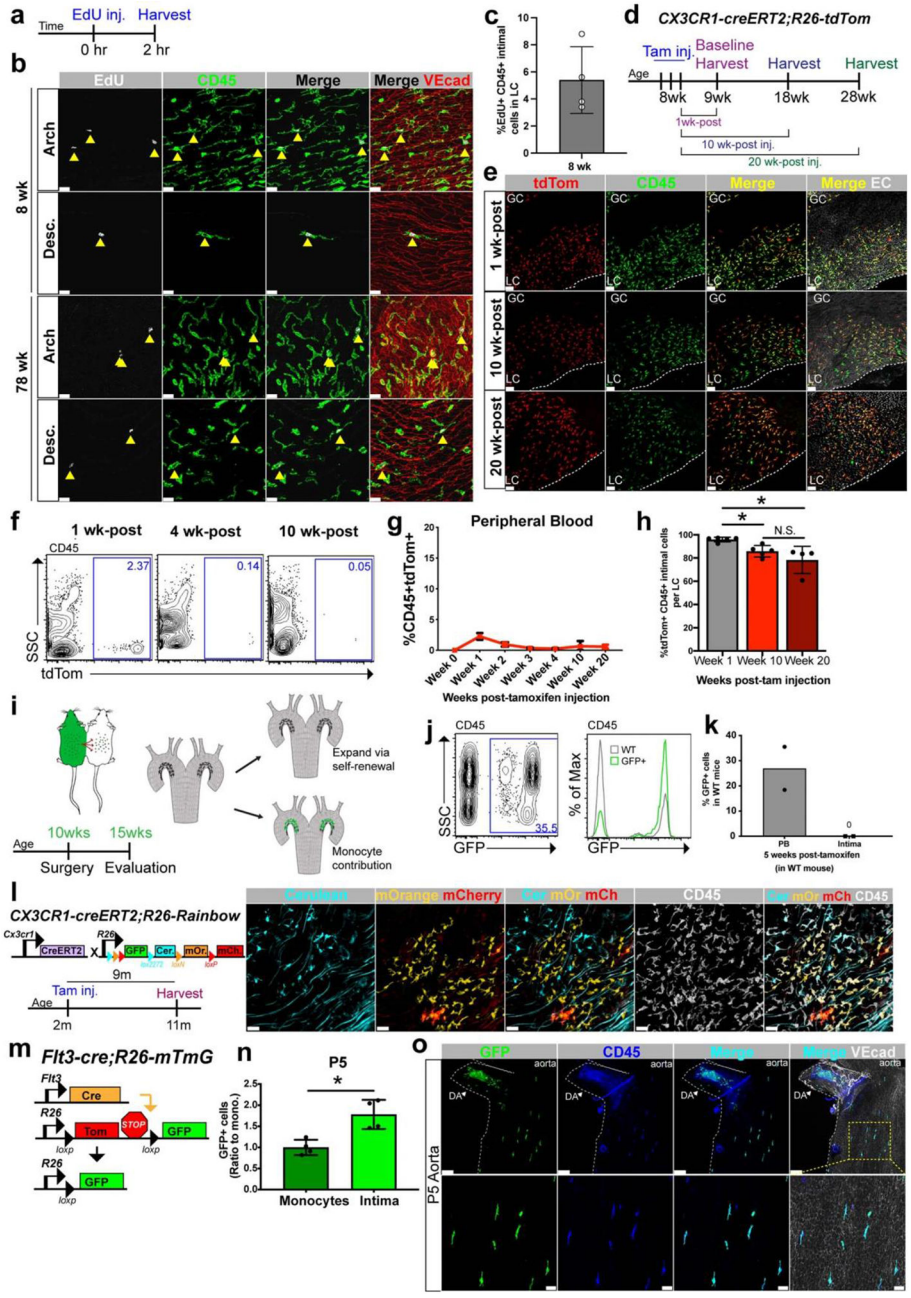

Extended Data Fig. 6: Aortic intimal macrophages are a self-replicating cell population of the tunica intima residing in areas of disturbed flow.

a, Timeline of 5-ethynyl-2′-deoxyuridine (EdU) incorporation. 8wk and 78wk old mice were injected with EdU and harvested 2-hrs later. **b**, EdU + (white) and CD45 + (green) co-expressing cells (yellow arrowheads) (arch and descending=Desc.). Scale bar, 20μm, n = 3 (78wk), 8 (8wk) mice. **c**, Intimal EdU+ CD45 + cells found in LC at 8wk (n = 4mice, ± SD). **d**, Experimental design for lineage tracing. 8wk old Cx3cr1^{creERT2};R26^{tdTomato} mice were pulse-labeled by Tam injection (inj.). Mice were harvested at 1wk-post-tam to establish reporter baseline. Evaluation was done at 10- and 20-wks post-tam. **e**, Images of CD45 (green) and tdTomato+ at 1-, 10-, and 20-wks post-tamoxifen. Endothelial

cell (EC) labeled with VE-cadherin (1- and 10-wk) and ERG (20-wk). Scale bar, 80μm; n = 4 (20wk), 5 (1wk,10wk) mice. GC = greater curvature. **f**, Representative fluorescence activated cell sorting (FACS) plot of tdTomato + / CD45 in the peripheral blood of $Cx3cr1^{creERT2}$;$R26^{tdTomato}$ mice weeks after tamoxifen injection. **g**, Percentage of peripheral blood positive for tdTomato during the time course of the study post-tamoxifen measured by flow cytometry (n = 3 (2wk, 3wk, 4wk,10wk), 5(20wk), and 6 (1wk) mice, ±SD). **h**, Percentage of intimal tdTomato+CD45 + cells found the aortic arch (LC) of $Cx3cr1^{creERT2}$;$R26^{tdTomato}$ mice at 1-, 10-, and 20-wks post-tamoxifen injection (n = 4 (20wk), 5 (1wk, 10wk) mice, Mann-Whitney *t*-test, ± SD, p = 0.0159 (1wk vs 10wk), p = 0.0159 (1wk vs 20wk), two-tailed, *p ≤ 0.05). **i**, Experimental design and timeline indicating the possible outcomes of the parabiosis experiment. GFP + and wild-type (WT) mice were surgically paired together to share chimeric circulation for 5wks prior to analyses. **j**, Representative FACS plot and histogram showing blood chimerism after parabiosis. **k**, Quantification of intimal GFP + CD45 + cells found in the LC of the WT mice (n = 2 pairs of mice, ± SD). PB = peripheral blood; WT = wild-type. **l**, Clonal tracing model, design, and possible outcomes. 2month old $Cx3cr1^{creERT2}$;$R26^{Rainbow}$ were administered a single dosage of tamoxifen. At 11months (9 months later), aortae were evaluated clonal expansion and retention of labeling of Mac^{AIRs} overtime. Images revealed clones of Mac^{AIRs} labeled and CD45 (white) 9months after tamoxifen labeling. Scale bar, 30μm; n = 4 mice. Cerulean (Cer), mOrange (mOr), mCherry (mCh). **m**, Lineage tracing ($Flt3^{cre}$;$R26^{mTmG}$) that labels cells derived from definitive hematopoiesis. Flt3-driven cre recombinase (cre) expression leads to an irreversible switch from Tomato (tom) to GFP expression in Flt3-expressing cells. As this is an irreversible switch, progeny will also be labeled GFP. **n**, GFP expression in CD45 + cells of P5 $Flt3^{cre}$;$R26^{mTmG}$ aortae relative to circulating monocytes from the same mice (n = 4 mice, Mann-Whitney *t*-test, ± SD, p = 0.0286, *p ≤ 0.05). **o**, Images of P5 $Flt3^{cre}$;$R26^{mTmG}$ aortae showing GFP expression (green) of intimal CD45 + (blue) cells exiting the ductus arteriosus (DA) (n = 4 mice).

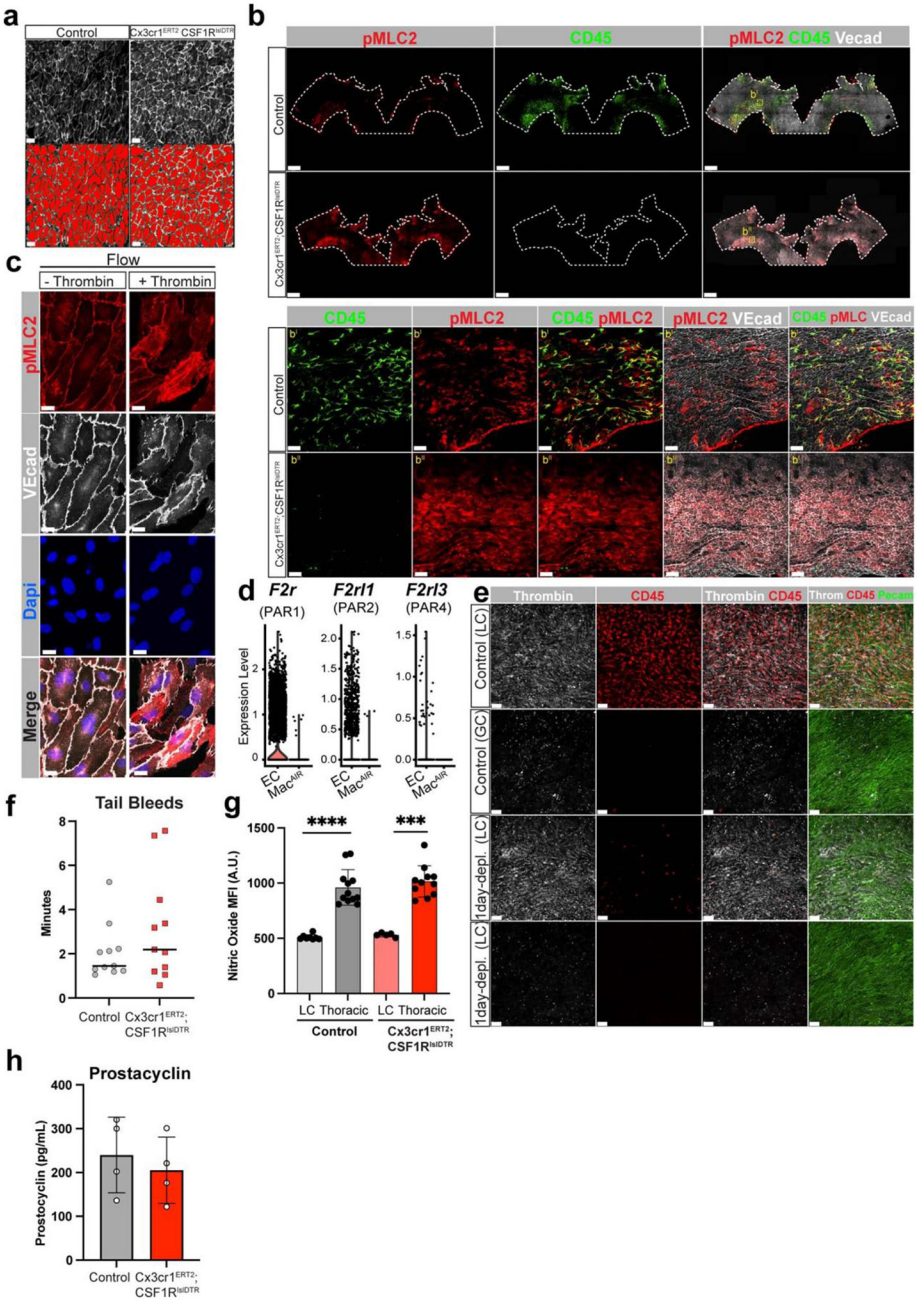

Extended Data Fig. 7: Thrombin distribution and signaling in areas of disturbed flow.

a, VE-cadherin (white) of control and macrophage-depleted ($Cx3cr1^{creERT2}$;$CSF1R^{lslDTR}$) aortae (upper panel). Changes in cell area and cell number were quantified by filling in red the area limited by VE-Cadherin staining. Note changes in shape and in cell number upon deletion of Mac^{AIRs} Scale bar, 15μm, n = 3 (control) or 4 ($Cx3cr1^{creERT2}$;$CSF1R^{lslDTR}$) mice. **b**, Low (upper panels) and high (lower panels) magnifications of control and $Cx3cr1^{creERT2}$;$CSF1R^{lsl}$DTR aortae staining for phosphorylation of myosin light chain 2 (pMLC2) (in red) and CD45 (green) one day post-diphtheria (DTx) toxin injection. Scale bar, 500μm (upper panels), 50μm (lower panels); n = 5 mice per group. **c**, Effect of thrombin

on human aortic endothelial cells (HAECs) pMLC2 (red) cultured under laminar flow. VE-cadherin (white) provides information on cell shape. DAPI (blue). Scale bar, 10μm. **d**, *F2r* (PAR1), *F2rl1* (PAR2), and *F2rl3* (PAR4) expression in endothelial cells (EC) and in Mac^{AIRs} from the arch scRNAseq data sets (Extended Data Fig. 2). **e**, En face images of the lesser curvature (LC) and greater curvature (GC) staining for thrombin (white) in control and $Cx3cr1^{creERT2}$;$CSF1R^{lsl DTR}$ aortae one-day after DTx (Scale bar, 50μm). **f**, Time of hemostatic plug formation measured following transverse amputation of the tip of the tail (3 mm) to assess hemostasis function in control and $Cx3cr1^{creERT2}$;$CSF1R^{lsl DTR}$ mice one-day post-DTx injection (n = 11 mice per group). **g**, *Ex vivo* mean fluorescent intensity (MFI) measurements of nitric oxide in the lesser curvature (LC) and thoracic aorta from control and $Cx3cr1^{creERT2}$;$CSF1R^{lsl DTR}$ mice one-day post-DTx injection (n = 2 mice per group and 3-7 number of areas quantified per mouse; Mann-Whitney *T*-test, ± SD, p = 0.0005, two-tailed ****p ≤ 0.0001). DAF-FM Diacetate (4-Amino-5-Methylamino-2',7'-Difluorofluorescein Diacetate) was used to detect and quantify NO. **h**, Plasma levels of prostacyclin in control and $Cx3cr1^{creERT2}$;$CSF1R^{lsl DTR}$ one-day post-DTx injection, measured by ELISA. No statistically significant changes noted (n = 4 mice per group, Mann-Whitney *t*-test, ± SD).

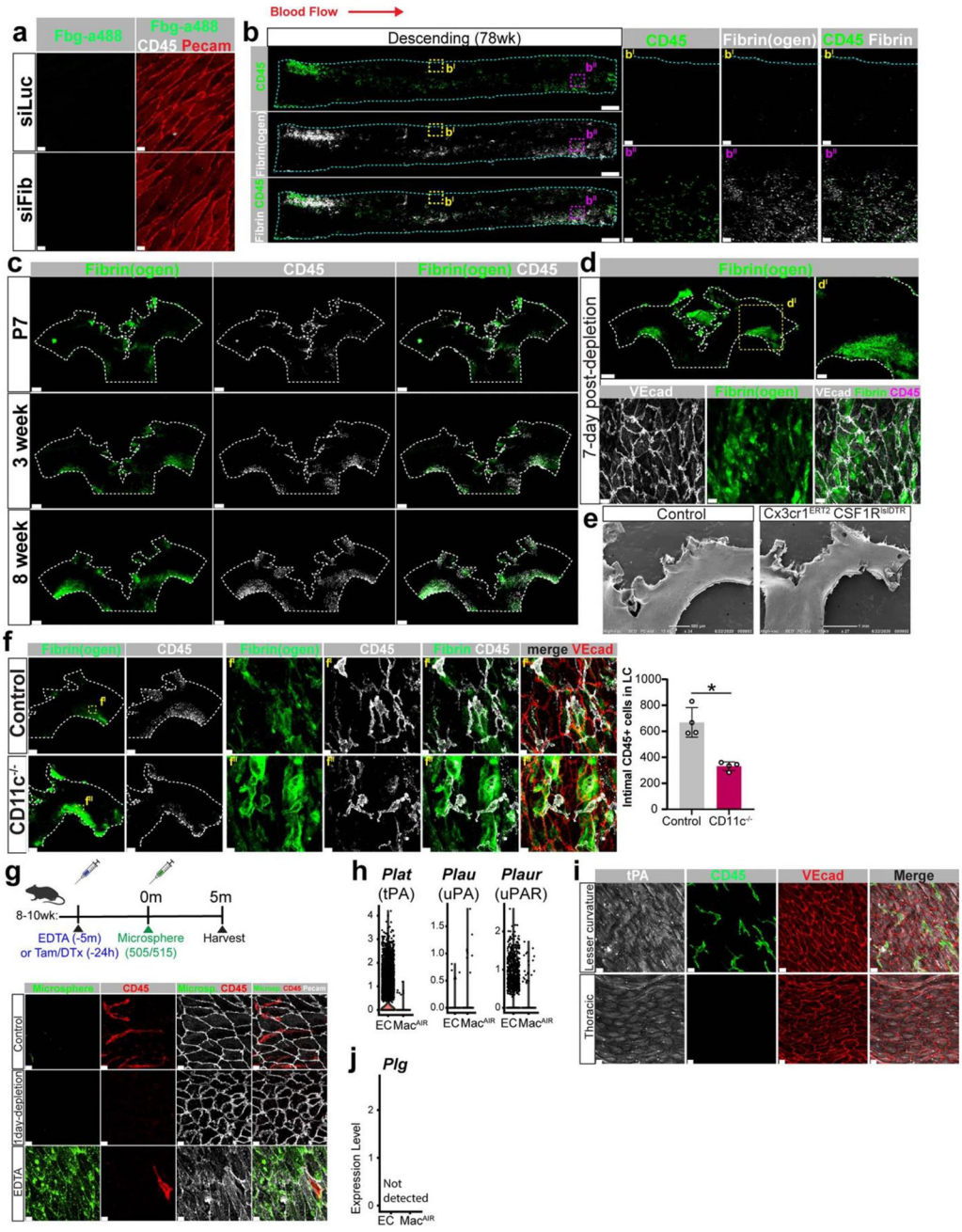

Extended Data Fig. 8: Mac^{AIRs} are necessary to prevent fibrin accumulation in areas of turbulent flow.

a, Images of the greater curvature after treatment with siFibrinogen or siLuciferase (control) for 7 days and then exposed to Fbg-a488 intravenously for 3 hrs. No fibrinogen binds to the greater curvature (unlike Fig. 5f). Scale bar, 7μm; n = 4 mice per group. **b**, Descending aortae (78wk old) stained for fibrin(ogen) (white) and CD45 (green). Higher magnifications in b^{I} and b^{II}, right panels. Scale bars, 1000μm and 100μm (b^{I-II}), n = 3 mice. **c**, Time-course of fibrin(ogen) (in green) and CD45 (white) at P7 (n = 3 mice), 3wk (n = 5 mice), and 8wk (n = 20 mice) old mice. Scale bar, 300μm. **d**, Fibrin(ogen) (green) in Cx3cr1^{creERT2};CSF1R^{lsl}DTR 7-days post-macrophage depletion. Scale bar, 500μm, 150μm

(d^{I}), and 8μm (bottom row). **e**, Scanning electron microscopy of aortae from control and Cx3cr1^{creERT2};CSF1R^{lsl}DTR 14-days post-macrophage depletion (n = 3 mice per group). **f**, Images of the aortic arch comparing fibrin(ogen) (green) and CD45 (white) in Control and CD11c$^{-/-}$ mice (Scale bar, 300μm and 8μm, n = 4 mice per group). Higher magnifications (**f^{I} and f^{II}**) on the right. Graph with number of CD45 + cells in the LC of control and CD11c$^{-/-}$ mice. (n = 4 mice per group, Mann-Whitney T-test, ± SD, p = 0.0286, two-tailed, *p ≤ 0.05). **g**, Schema of littermate control (negative control) and Cx3cr1^{creERT2};CSF1R^{lsl}DTR that received Tam/DTx (24 hr prior) and C57BL/6 EDTA treated mice (positive control). High magnification shown below. VE-Cadherin (white), CD45 (red) (Scale bar, 7μm; n = 3 mice per group). **h**, *Plat* (tPA), *Plau* (urokinase), *and Plaur* (urokinase receptor) expression in endothelial cells (EC) and Mac^{AIRs} from data sets in Extended Data Fig. 2. **i**, Immunostaining for tPA (white) in the LC and in the thoracic aorta in relation to CD45 (green). Endothelial cells (red) (Scale bar, 10μm; n = 3 mice). **j**, Expression of plasminogen (Plg) undetected in EC and Mac^{AIRs} by scRNA-seq.

Supplementary Material

Refer to Web version on PubMed Central for supplementary material.

ACKNOWLEDGEMENTS

We are grateful to Gwedalyn Randolph and Jesse Williams for the extensive discussions about intima resident macrophages and for the generous transfer of the *Cx3cr1^{creERT};CSF1R^{lsl}DTR* transgenic mouse. We are also thankful to William Mueller for Pecam1 antibodies. We are thankful to Karen Ridge for the generous transfer of the *Vimentin−/−* mice. We also would like to thank the Broad Stem Cell Research Center (BSCRC) and Jonsson Comprehensive Center (JCC) at UCLA for sequencing of scRNAseq libraries; the BSCRC flow core at UCLA and the Robert H. Lurie Comprehensive Cancer Center (RHLCCC) flow core at Northwestern University (NU), Feinberg School of Medicine; the Mouse Histology and Phenotyping core at NU; and the Center for Advanced Microscopy at NU. A special thanks to Michelle Steel and Snezana Mirkov for managing animal colonies and for assistance with husbandry and animal experiments. Additionally, thank you to Samuel Buchanan for help with cell size quantifications. We would also like to thank Farida V. Korobova from the Center for Advanced Microscopy at NU for support with the Scanning Electron Microscopy. We thank the members of the Arispe lab and the Feinberg Cardiovascular and Renal Research Institute at Northwestern University for extensive discussions. Illustrations were created with BioRender.com.

SOURCES OF FUNDING

This work was supported by R35HL140014 to M.L. Iruela-Arispe and Howard Hughes Medical Institute Gilliam Fellowship (GT11560) to Gloria Hernandez. JS is supported by Northwestern University Molecular and Translational Cardiovascular Training Program (T32HL134633; SP0040691). DAL is supported by NIH/NICHD training grant T32HD007491.

REFERENCES

1. Diacovo TG, Roth SJ, Buccola JM, Bainton DF & Springer TA Neutrophil rolling, arrest, and transmigration across activated, surface-adherent platelets via sequential action of P-selectin and the beta 2-integrin CD11b/CD18. Blood 88, 146–157 (1996). [PubMed: 8704169]
2. Ley K, Laudanna C, Cybulsky MI & Nourshargh S Getting to the site of inflammation: the leukocyte adhesion cascade updated. Nat. Rev. Immunol 7, 678–689 (2007). [PubMed: 17717539]
3. Liew PX & Kubes P The neutrophil's role during health and disease. Physiol. Rev 99, 1223–1248 (2019). [PubMed: 30758246]
4. Mamdouh Z, Chen X, Pierini LM, Maxfield FR & Muller WA Targeted recycling of PECAM from endothelial surface-connected compartments during diapedesis. Nature 421, 748–753 (2003). [PubMed: 12610627]

5. Gisterå A & Hansson GK The immunology of atherosclerosis. Nat. Rev. Nephrol 13, 368–380 (2017). [PubMed: 28392564]
6. Quintar A et al. Endothelial protective monocyte patrolling in large arteries intensified by western diet and atherosclerosis. Circ. Res 120, 1789–1799 (2017). [PubMed: 28302649]
7. Libby P, Nahrendorf M & Swirski FK Leukocytes link local and systemic inflammation in ischemic cardiovascular disease: an expanded “cardiovascular continuum”. J. Am. Coll. Cardiol 67, 1091–1103 (2016). [PubMed: 26940931]
8. Robbins CS et al. Local proliferation dominates lesional macrophage accumulation in atherosclerosis. Nat. Med 19, 1166–1172 (2013). [PubMed: 23933982]
9. Ross R Rous-Whipple Award Lecture. Atherosclerosis: a defense mechanism gone awry. Am. J. Pathol 143, 987–1002 (1993). [PubMed: 8214014]
10. Auffray C et al. Monitoring of blood vessels and tissues by a population of monocytes with patrolling behavior. Science 317, 666–670 (2007). [PubMed: 17673663]
11. Carlin LM et al. Nr4a1-dependent Ly6C(low) monocytes monitor endothelial cells and orchestrate their disposal. Cell 153, 362–375 (2013). [PubMed: 23582326]
12. Hanna RN et al. Patrolling monocytes control tumor metastasis to the lung. Science 350, 985–990 (2015). [PubMed: 26494174]
13. Choi J-H et al. Identification of antigen-presenting dendritic cells in mouse aorta and cardiac valves. J. Exp. Med 206, 497–505 (2009). [PubMed: 19221394]
14. Jongstra-Bilen J et al. Low-grade chronic inflammation in regions of the normal mouse arterial intima predisposed to atherosclerosis. J. Exp. Med 203, 2073–2083 (2006). [PubMed: 16894012]
15. Williams JW et al. Limited proliferation capacity of aortic intima resident macrophages requires monocyte recruitment for atherosclerotic plaque progression. Nat. Immunol 21, 1194–1204 (2020). [PubMed: 32895539]
16. Broadhouse KM et al. Assessment of PDA shunt and systemic blood flow in newborns using cardiac MRI. NMR Biomed. 26, 1135–1141 (2013). [PubMed: 23412748]
17. Colucci-Guyon E et al. Mice lacking vimentin develop and reproduce without an obvious phenotype. Cell 79, 679–694 (1994). [PubMed: 7954832]
18. Salvador J et al. Transcriptional evaluation of the ductus arteriosus at the single-cell level uncovers a requirement for vimentin for complete closure. Preprint at bioRxiv. doi:10.1101/2021.10.30.466605
19. Ma F, Hernandez GE, Romay M & Iruela-Arispe ML Single-cell RNA sequencing to study vascular diversity and function. Curr Opin Hematol (2021). doi:10.1097/MOH.0000000000000651
20. McDonald AI et al. Endothelial Regeneration of Large Vessels Is a Biphasic Process Driven by Local Cells with Distinct Proliferative Capacities. Cell Stem Cell 23, 210–225.e6 (2018). [PubMed: 30075129]
21. Ensan S et al. Self-renewing resident arterial macrophages arise from embryonic CX3CR1(+) precursors and circulating monocytes immediately after birth. Nat. Immunol 17, 159–168 (2016). [PubMed: 26642357]
22. Chakarov S et al. Two distinct interstitial macrophage populations coexist across tissues in specific subtissular niches. Science 363, (2019).
23. Lim HY et al. Hyaluronan Receptor LYVE-1-Expressing Macrophages Maintain Arterial Tone through Hyaluronan-Mediated Regulation of Smooth Muscle Cell Collagen. Immunity 49, 326–341.e7 (2018). [PubMed: 30054204]
24. Hernandez GE & Iruela-Arispe ML The many flavors of monocyte/macrophage--endothelial cell interactions. Curr Opin Hematol 27, 181–189 (2020). [PubMed: 32167947]
25. Tabula Muris Consortium et al. Single-cell transcriptomics of 20 mouse organs creates a Tabula Muris. Nature 562, 367–372 (2018). [PubMed: 30283141]
26. Satpathy AT et al. Zbtb46 expression distinguishes classical dendritic cells and their committed progenitors from other immune lineages. J. Exp. Med 209, 1135–1152 (2012). [PubMed: 22615127]
27. Epelman S, Lavine KJ & Randolph GJ Origin and functions of tissue macrophages. Immunity 41, 21–35 (2014). [PubMed: 25035951]

28. Ginhoux F & Guilliams M Tissue-Resident Macrophage Ontogeny and Homeostasis. Immunity 44, 439–449 (2016). [PubMed: 26982352]
29. Serbina NV & Pamer EG Monocyte emigration from bone marrow during bacterial infection requires signals mediated by chemokine receptor CCR2. Nat. Immunol 7, 311–317 (2006). [PubMed: 16462739]
30. Boyer SW, Schroeder AV, Smith-Berdan S & Forsberg EC All hematopoietic cells develop from hematopoietic stem cells through Flk2/Flt3-positive progenitor cells. Cell Stem Cell 9, 64–73 (2011). [PubMed: 21726834]
31. Epelman S et al. Embryonic and adult-derived resident cardiac macrophages are maintained through distinct mechanisms at steady state and during inflammation. Immunity 40, 91–104 (2014). [PubMed: 24439267]
32. Mehta D & Malik AB Signaling mechanisms regulating endothelial permeability. Physiol. Rev 86, 279–367 (2006). [PubMed: 16371600]
33. Rigor RR, Shen Q, Pivetti CD, Wu MH & Yuan SY Myosin light chain kinase signaling in endothelial barrier dysfunction. Med Res Rev 33, 911–933 (2013). [PubMed: 22886693]
34. Austin KM, Covic L & Kuliopulos A Matrix metalloproteases and PAR1 activation. Blood 121, 431–439 (2013). [PubMed: 23086754]
35. Hou H-H et al. MMP-12 activates protease-activated receptor-1, upregulates placenta growth factor, and leads to pulmonary emphysema. Am. J. Physiol. Lung Cell Mol. Physiol 315, L432–L442 (2018). [PubMed: 29722565]
36. Jaffré F, Friedman AE, Hu Z, Mackman N & Blaxall BC β-adrenergic receptor stimulation transactivates protease-activated receptor 1 via matrix metalloproteinase 13 in cardiac cells. Circulation 125, 2993–3003 (2012). [PubMed: 22610965]
37. Willis Fox O & Preston RJS Molecular basis of protease-activated receptor 1 signaling diversity. J. Thromb. Haemost 18, 6–16 (2020). [PubMed: 31549766]
38. Kulkarni JA, Witzigmann D, Chen S, Cullis PR & van der Meel R Lipid Nanoparticle Technology for Clinical Translation of siRNA Therapeutics. Acc. Chem. Res 52, 2435–2444 (2019). [PubMed: 31397996]
39. Bugge TH et al. Loss of fibrinogen rescues mice from the pleiotropic effects of plasminogen deficiency. Cell 87, 709–719 (1996). [PubMed: 8929539]
40. Prasad JM et al. Mice expressing a mutant form of fibrinogen that cannot support fibrin formation exhibit compromised antimicrobial host defense. Blood 126, 2047–2058 (2015). [PubMed: 26228483]
41. Motley MP et al. A CCR2 macrophage endocytic pathway mediates extravascular fibrin clearance in vivo. Blood 127, 1085–1096 (2016). [PubMed: 26647393]
42. Bonnardel J et al. Stellate cells, hepatocytes, and endothelial cells imprint the kupffer cell identity on monocytes colonizing the liver macrophage niche. Immunity 51, 638–654.e9 (2019). [PubMed: 31561945]
43. Sakai M et al. Liver-Derived Signals Sequentially Reprogram Myeloid Enhancers to Initiate and Maintain Kupffer Cell Identity. Immunity 51, 655–670.e8 (2019). [PubMed: 31587991]
44. Scott CL et al. Bone marrow-derived monocytes give rise to self-renewing and fully differentiated Kupffer cells. Nat. Commun 7, 10321 (2016). [PubMed: 26813785]
45. Colvin RB & Dvorak HF Fibrinogen/fibrin on the surface of macrophages: detection, distribution, binding requirements, and possible role in macrophage adherence phenomena. J. Exp. Med 142, 1377–1390 (1975). [PubMed: 1104745]
46. Hiller O, Lichte A, Oberpichler A, Kocourek A & Tschesche H Matrix metalloproteinases collagenase-2, macrophage elastase, collagenase-3, and membrane type 1-matrix metalloproteinase impair clotting by degradation of fibrinogen and factor XII. J. Biol. Chem 275, 33008–33013 (2000). [PubMed: 10930399]
47. Motterle A et al. Influence of matrix metalloproteinase-12 on fibrinogen level. Atherosclerosis 220, 351–354 (2012). [PubMed: 22119538]
48. Tardif G, Reboul P, Pelletier J-P & Martel-Pelletier J Ten years in the life of an enzyme: the story of the human MMP-13 (collagenase-3). Mod Rheumatol 14, 197–204 (2004). [PubMed: 17143675]

49. Bugge TH, Flick MJ, Daugherty CC & Degen JL Plasminogen deficiency causes severe thrombosis but is compatible with development and reproduction. Genes Dev. 9, 794–807 (1995). [PubMed: 7705657]
50. Goguen JD, Bugge T & Degen JL Role of the pleiotropic effects of plasminogen deficiency in infection experiments with plasminogen-deficient mice. Methods 21, 179–183 (2000). [PubMed: 10816379]
51. Gomez Perdiguero E et al. Tissue-resident macrophages originate from yolk-sac-derived erythro-myeloid progenitors. Nature 518, 547–551 (2015). [PubMed: 25470051]
52. Hoeffel G et al. C-Myb(+) erythro-myeloid progenitor-derived fetal monocytes give rise to adult tissue-resident macrophages. Immunity 42, 665–678 (2015). [PubMed: 25902481]
53. Schulz C et al. A lineage of myeloid cells independent of Myb and hematopoietic stem cells. Science 336, 86–90 (2012). [PubMed: 22442384]
54. Yona S et al. Fate mapping reveals origins and dynamics of monocytes and tissue macrophages under homeostasis. Immunity 38, 79–91 (2013). [PubMed: 23273845]
55. Strilchuk AW et al. Sustained depletion of FXIII-A by inducing acquired FXIII-B deficiency. Blood 136, 2946–2954 (2020). [PubMed: 32678423]
56. Korsunsky I et al. Fast, sensitive and accurate integration of single-cell data with Harmony. Nat. Methods 16, 1289–1296 (2019). [PubMed: 31740819]
57. Ali SR et al. Developmental heterogeneity of cardiac fibroblasts does not predict pathological proliferation and activation. Circ. Res 115, 625–635 (2014). [PubMed: 25037571]
58. Navab M et al. Monocyte migration into the subendothelial space of a coculture of adult human aortic endothelial and smooth muscle cells. J. Clin. Invest 82, 1853–1863 (1988). [PubMed: 3198759]
59. Rinkevich Y, Lindau P, Ueno H, Longaker MT & Weissman IL Germ-layer and lineage-restricted stem/progenitors regenerate the mouse digit tip. Nature 476, 409–413 (2011). [PubMed: 21866153]

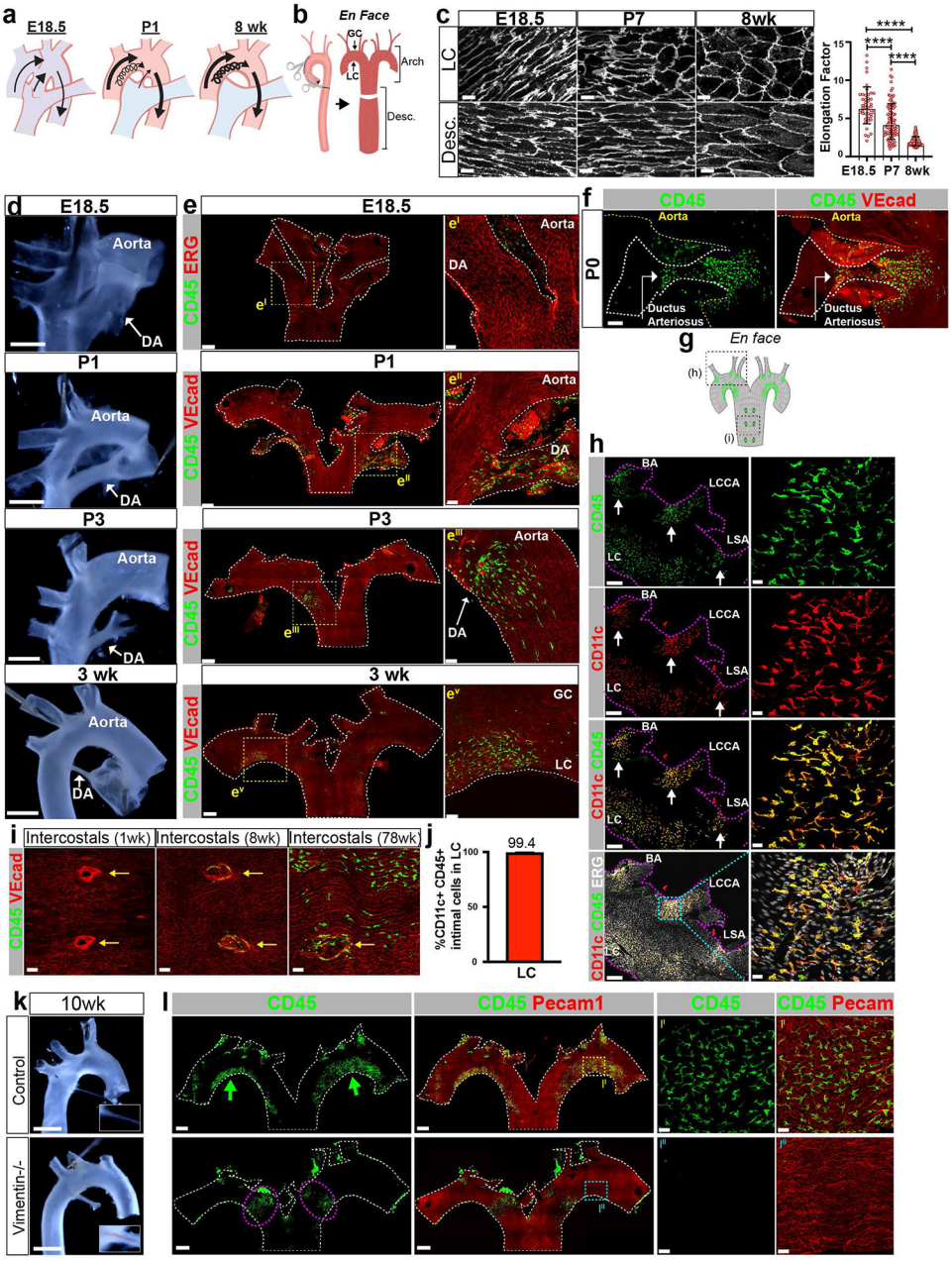

Figure 1. Hemodynamic changes associated with birth result in the recruitment of immune cells to the tunica intima

a, Anatomical and hemodynamic changes associated with birth. E18.5 blood from the pulmonary arteries mixes with blood from the aorta through the ductus arteriosus. P1, the ductus arteriosus constricts and this contributes to disturbed flow in the aortic arch. Shortly thereafter and in the adult (8wks), the aorta and the pulmonary artery are no longer connected. Red denotes highly levels of oxygen in the blood; while blue denotes lower oxygen in the blood; purple mixed levels of oxygen.

b, Schema illustrating the process of aorta dissection for whole mount observation of *en face* imaging. Greater Curvature (GC), Lesser Curvature (LC), Descending aorta (Desc).

c, Whole mount, *en face* images of the lesser curvature and of the descending aorta from E18.5, P7, and 8wk mice. Endothelial cells, through mechanosensation alter their shape in the lesser curvature from elongated to polygonal, consistent with disturbed and oscillatory flow of that region. The elongation factor in LC was calculated and shown on the adjacent graph (n=3-5 mice per time point, Mann-Whitney t-test, ± SD, ****$p \leq 0.0001$, Scale bar, 10μm).

d, Bright field images showing remodeling of the ductus arteriosus (DA) at the indicated developmental ages in C57BL/6 mice (Scale bars, E18.5, P1,P3= 500μm and 3wk=1000μm; n=5-10 per time point).

e, En face images show exit of immune cells from the DA and their migration to areas of disturbed flow at the indicated developmental ages. VE-Cad or ERG is shown in red. Scale bars, 300μm and 70μm ($e^{I\text{-}V}$), n=5-10 per time point.

f, Lumen of DA *en face* (dotted white lines) at P0 highlighting immune cells and their migration towards the aorta. Scale bar, 50μm, n=5.

g, Illustration of a dissected aorta highlighting regions of disturbed blood flow where intimal immune cells (green) accumulate in healthy, adult mice. Dotted black boxes indicate branch openings that are shown in the following panels (h,i).

h, *En face* images of large branch openings in the aortic arch of adult, C57BL/6 mice. Note accumulation of intimal myeloid (CD11c+ in red and CD45+ in green) cells (white arrows) in the anterior aspects of large branch openings. Co-distribution of CD45 and CD11c markers can be seen in most of the cells. ERG is shown in white to identify endothelial nuclei. Brachiocephalic trunk (BA) Left common carotid artery (LCCA), Left subclavian artery (LSA), lesser curvature (LC) of aortic arch. Scale bar, 200μm (left column) and 20μm (right column), n=15.

i, Time-course (1wk, 8 wk, 78wk) evaluation of intimal CD45+ cells (green) deposition in the opening of intercostal arteries (yellow arrows) of healthy, C57BL/6 mice. Note, no intimal CD45+ cells were found in 1wk old aortae. VE-Cad is shown in red. Additionally, 78wk aortae show intimal CD45+ cells residing in laminar shear regions of the descending aorta as well. Scale bar, 50μm, n=12 (1wk), n=498 (8wk), n=6 (78wk).

j, 99.4% of intimal CD45+ cells in the LC of the aortic arch are also labeled by CD11c+ (n=4, ± SD).

k, Bright field images of 10wk control and *Vimentin*$^{-/-}$ (*Vim*$^{-/-}$) aortae. Higher magnification shows the remnant (control) and patent ductus arteriosus (*Vim*$^{-/-}$). Note blood in the lumen of the DA in the *Vim*$^{-/-}$. (n=8, Scale bar, 1300μm).

l, *En face* images of the aortic arch of 10wk old control and *Vim*$^{-/-}$ mice, highlighting accumulation of immune cells in control (green arrows) and *Vim*$^{-/-}$ (dotted pink ovals). VE-Cad is shown in red. High magnification of the indicated squares is shown on the right panels ($l^{I\text{-}II}$). Scale bar, 500μm and 40μm ($l^{I\text{-}II}$).

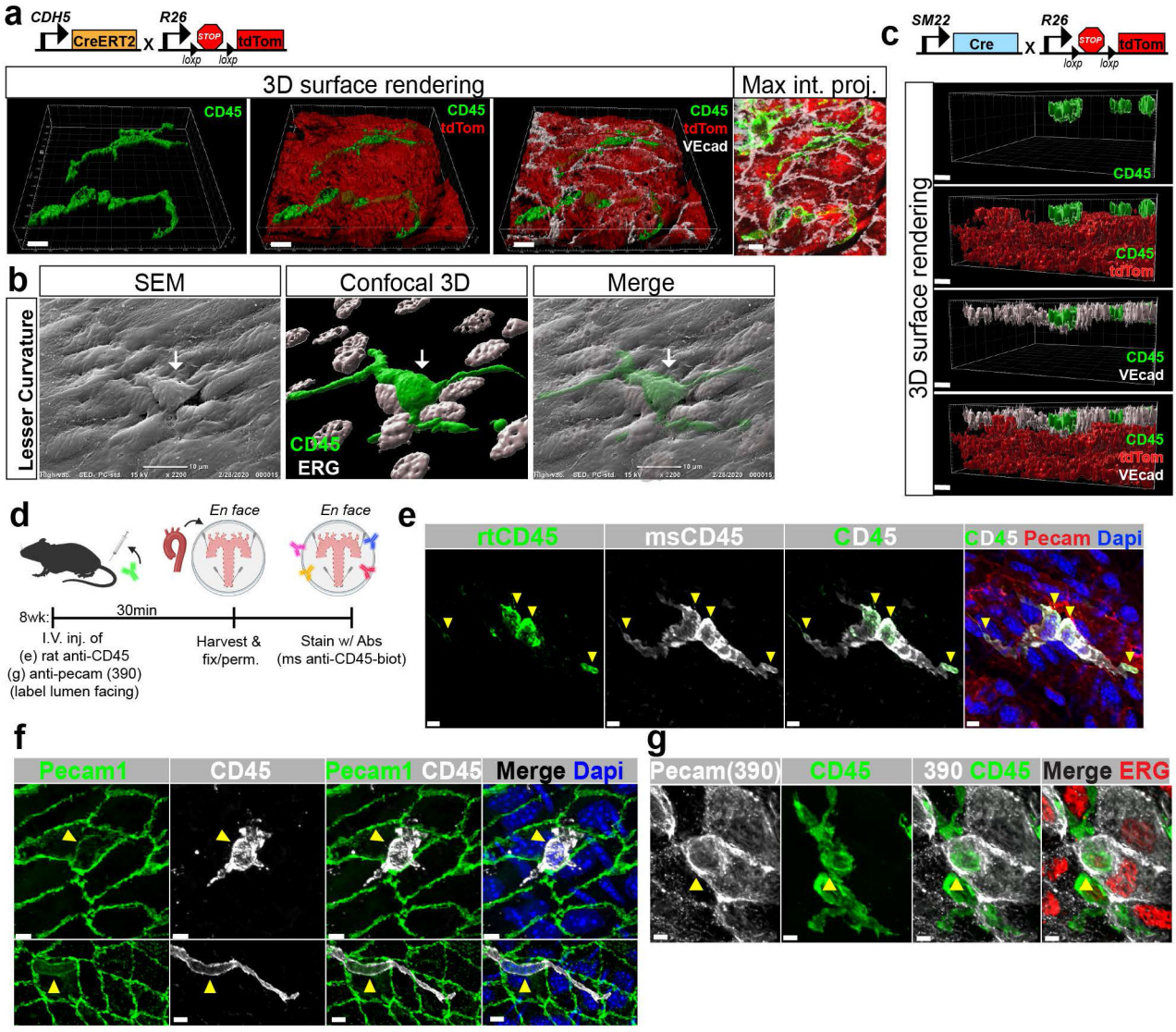

Figure 2. Topology of intimal myeloid cells in relation to the endothelium

a, $CDH5^{CreERT2}$;$R26^{tdTomato}$ construct of the mice used for 3D surface rendering of adult aortae to visualize the spatial location of intimal CD45+ cells (green) relative to the endothelium (tdTomato). VE-Cadherin is shown in white. Scale bars, 8μm, n=3.

b, Confocal and scanning electron microscopy (SEM) images of the same aorta overlaid to determine location of intimal CD45+ cells (green in confocal) in relation to the endothelium. ERG was used to visualize endothelial nuclei in the confocal images. Scale bar, 10μm, n=3.

c, $SM22^{cre}$;$R26^{tdtomato}$ construct of mice used for 3D rendering. Side view of 3D surface image of adult aortae to visualize spatial location of intimal CD45+ cells (green) relative to the vascular smooth muscle cells (tdTomato). Endothelial cells were visualized with VE-cadherin antibodies (white). Scale bars, 5μm, n=3.

d, Schema of experimental design related to panel **e** and **g**.Tail vein injection of (e) rat anti-CD45 antibody (detected in green) was followed by euthanasia and fixation of the aorta

30min later. Subsequent permeabilization and staining with an additional, distinct CD45 antibody (detected using far-red – labeled in white).

e, *En face* images of the experiment described. Yellow arrowheads indicate the portions of immune cells exposed to the lumen (green). In white is the identification of mouse anti-CD45 biotinalyated antibody labeled with strepaviden-a647 used in immunostaining post-permeabilization. Pecam-1 (in red) and DAPI (blue). Scale bar, 5μm, n=3.

f, *En face* images of the lesser curvature (LC) staining for Pecam-1 (green). Yellow arrowheads show faint Pecam-1positivity in CD45+ cells residing in the intima. Endothelial cells were detected in green with Pecam1. Scale bar, 5μm, n=6.

g, C57BL/6 mice were injected intravenously with non-blocking Pecam-1 (390) antibody to further examine exposure of cell bodies to the lumen. Mice were sacrificed and harvested 15mins post-injection. CD45 (in green) was used to identify immune cells and ERG (red) was used to identify endothelial cells. Yellow arrowheads indicate Pecam-1+ regions of the intimal immune cells. Scale bar, 4μm, n=3.

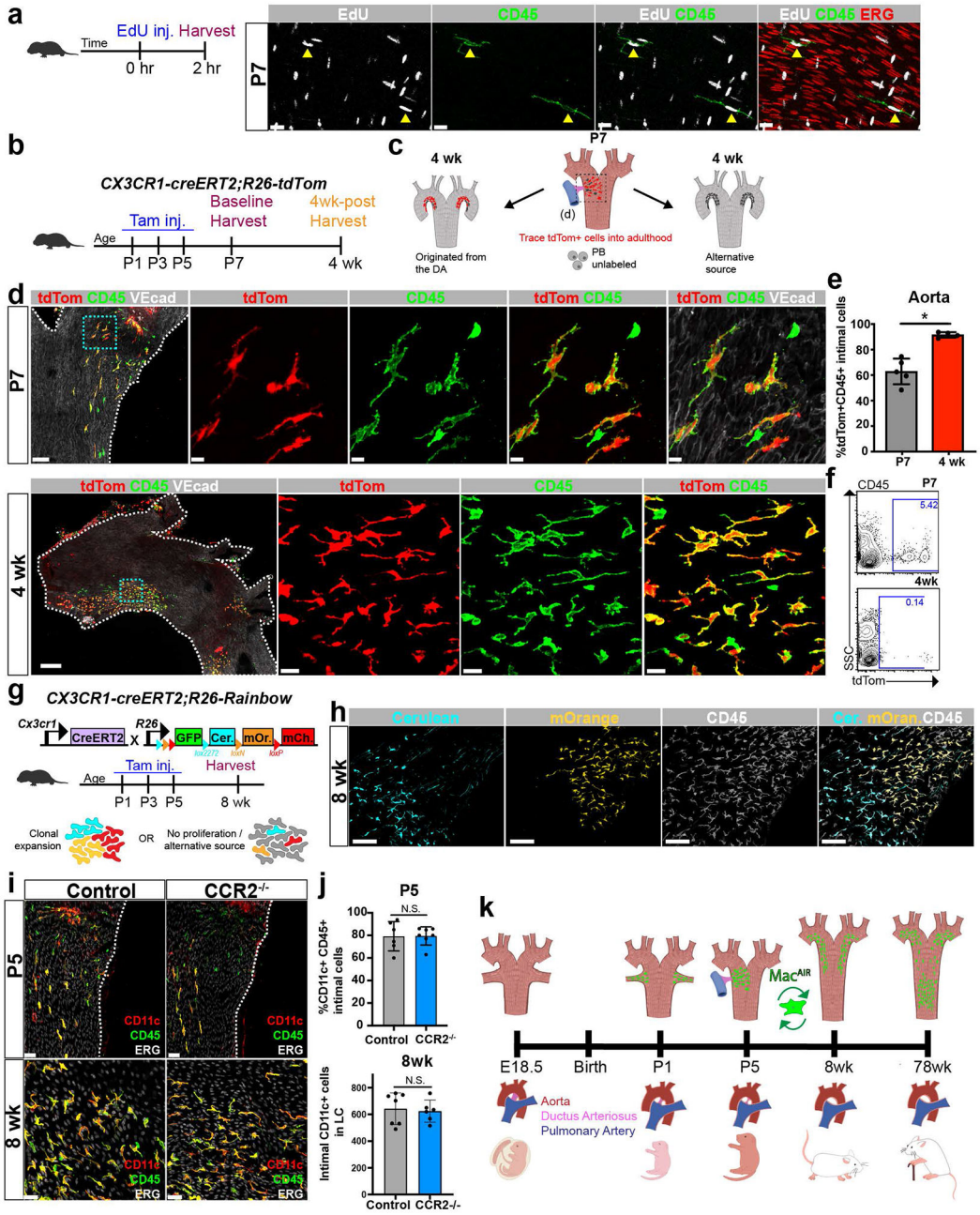

Figure 3. Aortic intimal macrophages seed the aorta immediately post-birth and self-renew in areas of oscillatory and disturbed flow

a, Schema of experimental design. Injection of EdU was applied to P7 mice 2hrs prior to euthanasia. Intimal CD45+ cells (in green) proliferate (EdU+ in white) *in situ* (yellow arrowheads). Endothelial cells were visualized with ERG (in red). Note, EdU+ CD45+ cells are negative for ERG. Scale bar, 20μm, n=3.

b, Lineage Tracing experimental design: $Cx3cr1^{creERT2}$;$R26^{tdTomato}$ neonates were administered tamoxifen at P1, P3, and P5. At P7, aortae were harvested from half of the litter to obtain a baseline control for normalization of reporter expression. At 4wks, aortae

were harvested from the remaining littermates to assess retention of reporter expression in Mac^{AIRs}.

c, Illustration depicting the possible outcomes of the experiment. Note, labeling of circulating blood cells tdTomato is negligible in this model (as per panel g). Peripheral blood (PB).

d, tdTomato+ intimal immune cells in P7 (top) and 4wk (bottom) aortae of $Cx3cr1^{creERT2}$;$R26^{tdTomato}$ post-neonatal tamoxifen administration. Note, Mac^{AIRs} in the lesser curvature of 4wk $Cx3cr1^{creERT2}$;$R26^{tdTomato}$ aortae retained reporter expression (tdTomato+) when labeled postnatally, as per comparison between P7 (baseline) and 4wks (lineage traced). Immune cells were visualized with CD45 (green), VE-Cad was used to visualize endothelial cells (white). Scale bar, 80μm and 10μm, n=5 (P7); 300μm and 20μm, n=4 (4wk).

e, Percentage of intimal tdTomato+ CD45+ cells in $Cx3cr1^{creERT2}$;$R26^{tdTomato}$ aortae at P7 and 4wk when labeled with tamoxifen post-natally (n=4-5 per timepoint, Mann-Whitney T-test, ± SD, *$p \leq 0.05$).

f, Representative FACS plots of tdTomato labeling in circulating blood cells at P7 and 4wks (n=3-4 per timepoint).

g, Clonal tracing model, experimental design, and possible outcomes. $Cx3cr1^{creERT2}$;$R26^{Rainbow}$ neonates were administered tamoxifen at P1, P3, and P5. At 8wks, aortae were harvested to evaluate clonal expansion and labeling of Mac^{AIRs}.

h, Clones of Mac^{AIRs} labeled with different fluorescent proteins at 8wk (initial tamoxifen injection at P1, P3 and P5). CD45+ cells were detected in white. Scale bar, 100μm; n=5.

i, *En face* images comparing intimal CD11c+CD45+ cells from control and $CCR2^{-/-}$ mice at P5 (top row, former ductus arteriosus region) and 8wk (bottom row, lesser curvature of aortic arch). CD11c (in red), CD45 (in green) and ERG (in white). Scale bar, 100μm and 50μm; n=6-7 per timepoint.

j, Comparison of intimal CD11c+CD45+ cells in control and $CCR2^{-/-}$ P5 aortae (n=6-7, Mann-Whitney T-test, ± SD) or in the lesser curvature of the aortic arch in 8wk aortae (n=6-7 per timepoint, Mann-Whitney T-test, ± SD).

k, Schematic summary of findings (from Figures 1-3). Intima-resident macrophages (Mac^{AIR}) enter the aorta via the ductus arteriosus immediately post-birth, expand through self-renewal and populate the lesser curvature of the aortic arch. Eventually with age, macrophages also accumulate in the descending aorta.

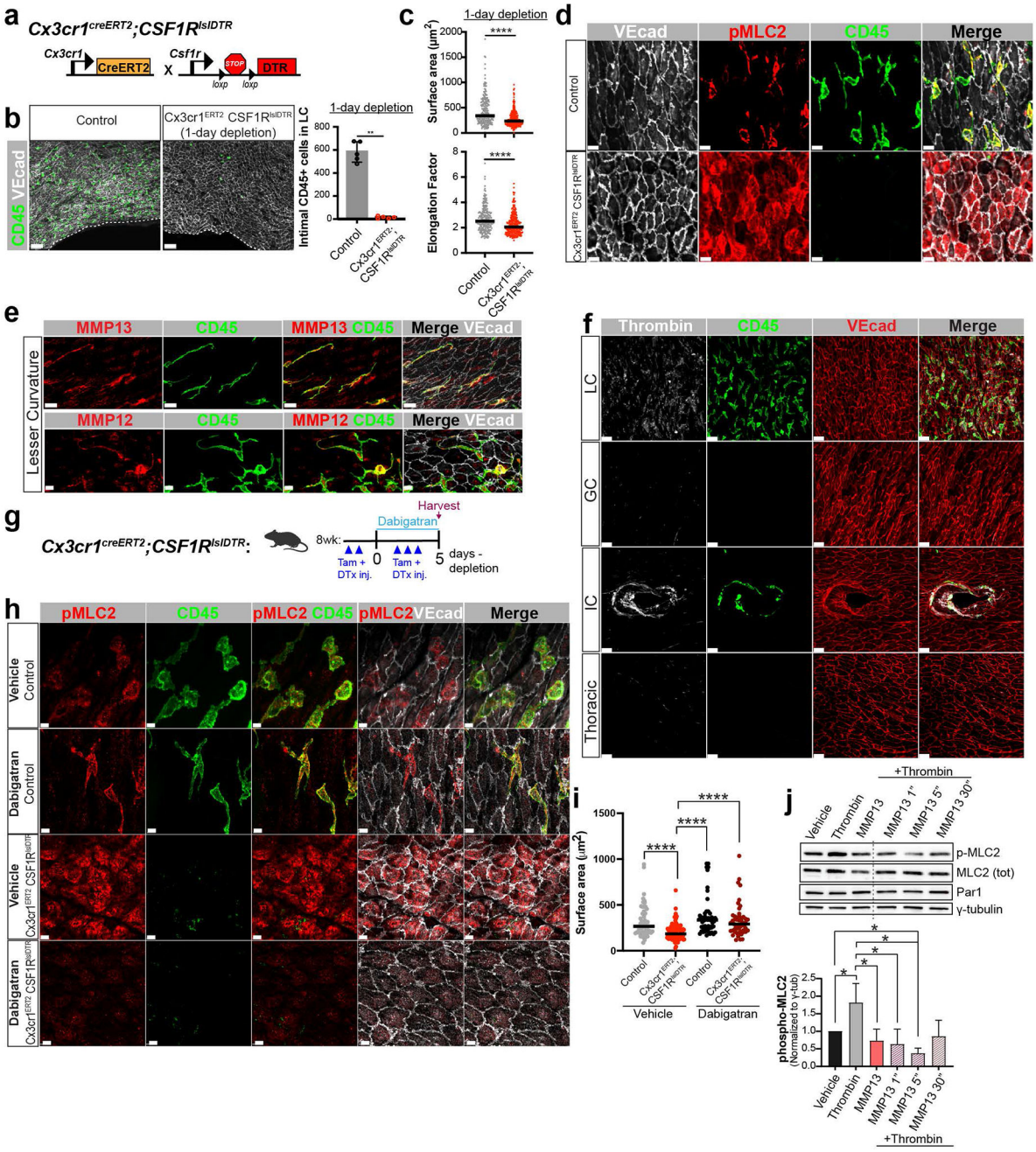

Figure 4. Mac^{AIRs} are essential to prevent thrombin-mediated endothelial cell contraction in regions of oscillatory and disturbed flow.

a, Schema of constructs used to deplete the Mac^{AIR} population. Inducible Mac^{AIR}-depletion model (Cx3cr1^{creERT2};CSF1R^{lslDTR}) requires treatment of both tamoxifen and diphtheria toxin to induce apoptosis on double positive cells. Diphtheria toxin receptor (DTR).

b, *En face* images and total number of intimal CD45+ cells in the lesser curvature (LC) of the aortic arch from littermates controls and Cx3cr1^{creERT2}; CSF1R^{lslDTR} mice that were exposed to post-tamoxifen and diphtheria toxin for 24hrs. Both control and experimental mice were injected with tamoxifen and diphtheria toxin. CD45+ (green) cells in the aorta

are nearly completely depleted by this approach. Scale bar, 50μm; n=5 per group, Mann-Whitney *T*-test, ± SD, **p ≤ 0.01.

c, Surface area and elongation factor measurements of endothelial cells in the lesser curvature of Cx3cr1^{creERT2};CSF1R^{lslDTR} and littermate controls post-Mac^{AIR} depletion in aortae. VE-cadherin staining was used to identify cell borders (n= 3-4 mice per group, Mann-Whitney T-test, ± SD, ****p ≤ 0.0001).

d, Phosphorylated-myosin light chain 2 (pMLC2) staining (red) in the lesser curvature of the aortic arch 1-day post-tamoxifen and diphtheria toxin injection in control and Cx3cr1^{creERT2};CSF1R^{lslDTR} mice. CD45 (green) and VE-Cadherin (in white). Scale bar, 10μm, n=5 per group.

e, *En face* images co-staining for MMP12 or MMP13 (red), CD45 (green), and VE-Cadherin (white). Note co-localization of MMP12 and 13 with CD45+ cells. Scale bar, 20μm and 10μm, n=3.

f, Concentration of thrombin in areas of oscillatory and disturb flow in 8wk old C57BL/6 aortae (lesser curvature (LC), greater curvature (GC), intercostal artery (IC), Scale bar, 20μm, n=3).

g-i Effects of Dabigatran on Cx3cr1^{creERT2};CSF1R^{lslDTR} and control aortae.

g, Experimental design. 8wk old Cx3cr1^{creERT2};CSF1R^{lslDTR} and littermate controls were injected with tamoxifen (Tam) and diphtheria toxin (DTx) to induce depletion of Mac^{AIRs}. Additionally, mice were treated with vehicle or Dabigatran for 5 days. Note, constant injection of tamoxifen and diphtheria toxin is needed to keep macrophages from re-populating the lesser curvature.

h, Representative *en face* images of the lesser curvature 5-days post-experimental manipulation as indicated. Immunocytochemistry included pMCL2 (red), CD45 (green) and (VE-Cadherin in white). Note the impressive loss of pMLC2 in dabigatron-treated Cx3cr1^{creERT2};CSF1R^{lslDTR} Mac^{AIR} depleted mice. Scale bar, 7μm, n=4-10 per group.

i, Surface area measurements of endothelial cells in the lesser curvature of Cx3cr1^{creERT2};CSF1R^{lslDTR} and littermate control 5-days post-dabigatran treatment (n=4-10 per group, Mann-Whitney T-test, ± SD, ****p ≤ 0.0001).

j, Western blot analysis of human aortic endothelial cells (HAECs) treated with Thrombin, MMP13, or pre-treated with MMP13 for 1min, 5min, and 30min and then additionally stimulated with Thrombin for 5 mins (n=4, Mann-Whitney T-test, ± SD, *p ≤ 0.05).

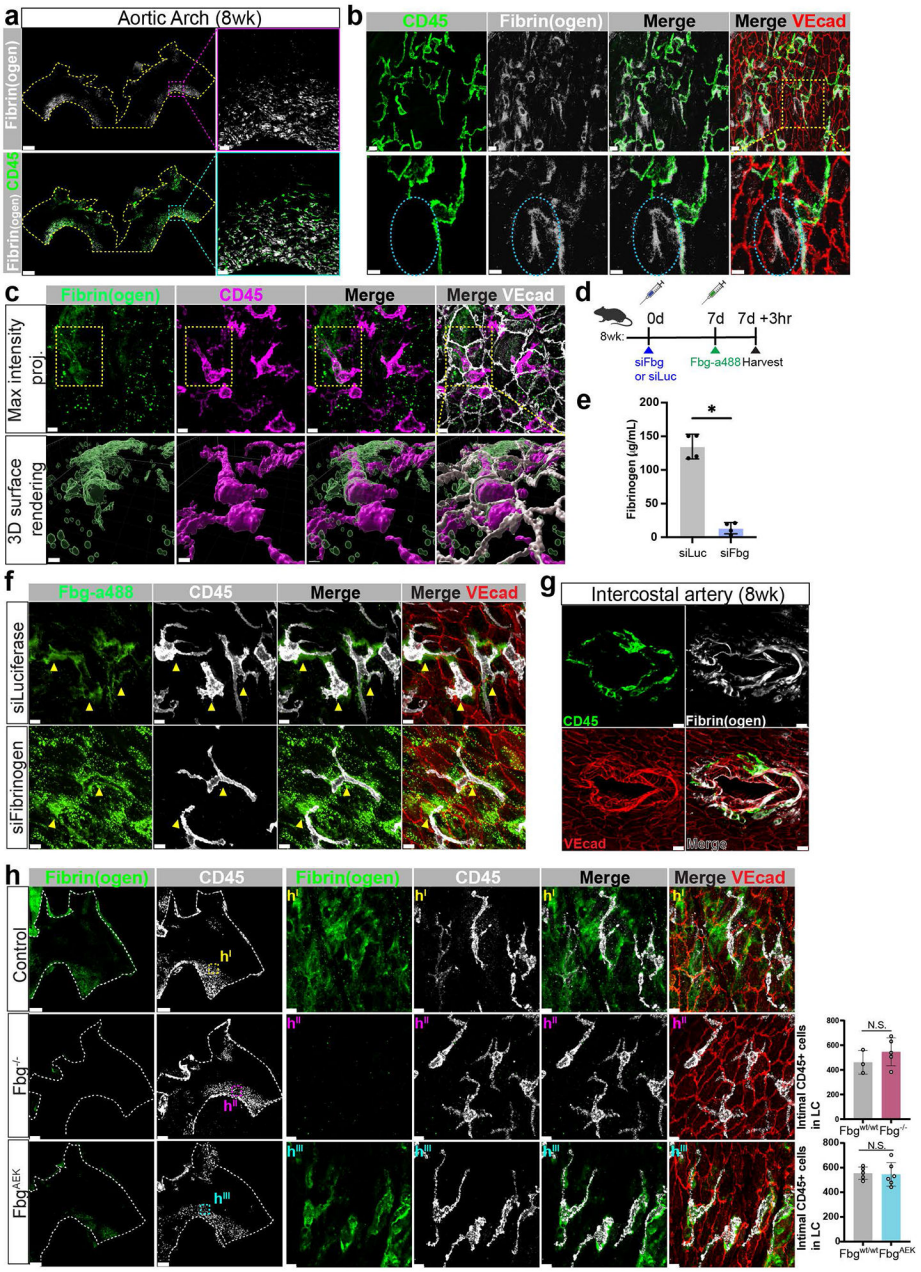

Figure 5. Fibrin(ogen) is deposited and binds to Mac^{AIRs} in regions that experience oscillatory and disturbed flow

a, Whole mount, *en face* images of fibrin(ogen) (white) and CD45+ cells (green) in the aortic arch of 8wk old C57BL/6 mice. Scale bar, 500μm and 50μm, n=20.

b, Fibrin(ogen) (white) was overlaid with CD45 staining (green) in adult aortic arch. Higher magnification (lower panel) of blue dotted insert highlights fibrin(ogen) staining in an area that resembles the cellular process of a Mac^{AIR} (blue dotted eclipse). Scale bar, 10μM and 5μM.

c, *En face* images of fibrin(ogen) location in the aortic arch displayed using max intensity projections (top row) and 3D surface rendering (bottom row). Scale bar, 7μm and 4μm, n=16.

d, Experimental design. 8wk old C57BL/6 mice were injected via tail vein with either siFibrinogen or siLuciferase (control). 7-days later, mice were tail vein injected with fibrinogen conjugated to a488 (fbg-a488). After 3 hours post-fbg-a488 injection, aortae were harvested for analysis.

e, Plasma levels of Fibrinogen 7-days post-mRNA injection, measured by ELISA (n=4 per group, Mann-Whitney T-test, ± SD, *p ≤ 0.05).

f, Distribution of intravenously injected fbg-a488 in relation to Mac^{AIRs}. CD45 (white). Yellow arrowheads indicate surface bound fbg-a488 to Mac^{AIRs} (n=4 per group, Scale bar, 4μm).

g, Adult (8wk) intercostal artery exhibiting fibrin(ogen) deposition (white) and intimal CD45+ cells accumulation (green). VE-Cadherin identifies endothelial cells in red. (Scale bar, 70μm, n=15).

h, *En face* images of the aortic arch comparing fibrin(ogen) accumulation (green) and immune cell (CD45, white) deposition in Control (h^{I}), fibrinogen−/− ($Fbg^{-/-}$, h^{II}), and $fibrinogen^{AEK}$ (Fbg^{AEK}, h^{III}). VE-Cadherin identifies endothelial cells in red. Scale bar, 300μm and 8μm, n=3-6. Adjacent graph represents the quantifications of Mac^{AIRs} in the lesser curvature of the aortic arch in $Fbg^{-/-}$ and Fbg^{AEK} mice compared to colony controls (n=3-6 per group, Mann-Whitney T-test, ± SD, *p ≤ 0.05).

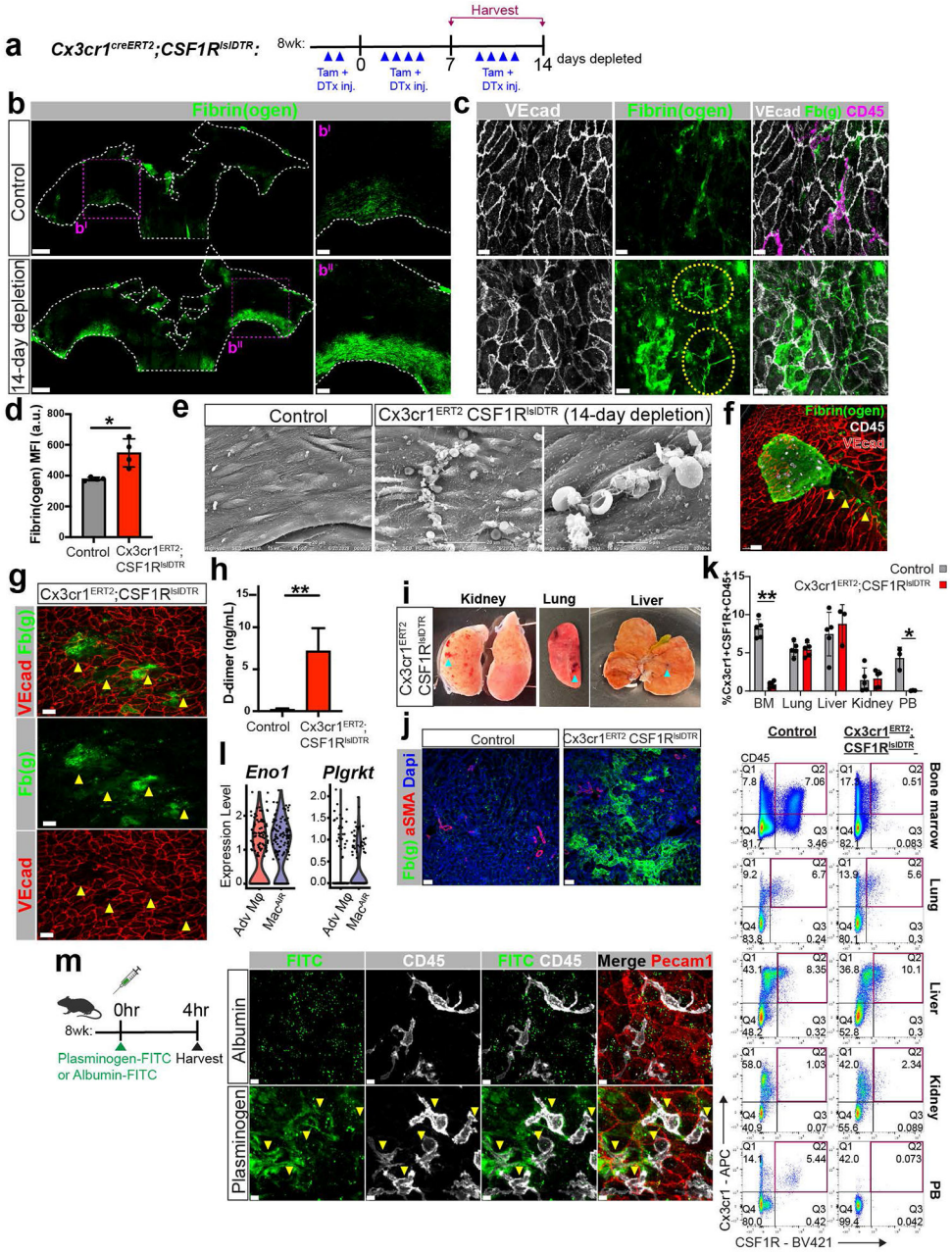

Figure 6. Mac^{AIRs} are necessary to clear fibrin deposits in regions of oscillatory and disturbed blood flow.

a, Experimental design schematic for long-term Mac^{AIR} depletion. Cx3cr1^{creERT2};CSF1R^{lslDTR} mice and littermate controls were injected every other day, alternating tamoxifen (Tam) and diphtheria toxin (DTx) for 14-days.

b, Increased accumulation of fibrin(ogen) (green) in the lesser curvature of aortae 14-days post-continued Mac^{AIR} depletion in Cx3cr1^{creERT2};CSF1R^{lslDTR} mice compared to littermate control (Scale bar, 500μm (B) and 150μm (b^{I-II}); n=4-11 per group).

c, Fibrin fibrils (green) observed in aortae 14-days of continued Mac^{AIR} depletion (yellow dotted ovals). VE-Cadherin identifies endothelial cells in white and CD45 is shown in pink (Scale bar, 10μm, n=4-11 per group).

d, Mean Fluorescence Intensity of Fibrin(ogen) in the lesser curvature of the aortic arch in Cx3cr1^{creERT2};CSF1R^{lslDTR} mice after 14-days of continuedMac^{AIR}depletion compared to littermate controls (n=4 per group, Mann-Whitney *T*-test, ± SD, *p ≤ 0.05).

e, *En face* scanning electron microscopy images showing microthrombi and fibrin accumulating in the lesser curvature of the aortic arch in Cx3cr1^{creERT2};CSF1R^{lslDTR} mice 14-days post-continued Mac^{AIR} depletion. Scale bar, 20μm and 5μm.

f, Microthrombi (green) and intima rupture (yellow arrowheads) of a Cx3cr1^{creERT2};CSF1R^{lslDTR} mouse that had to be euthanized due to declined health 7-days post-continued macrophage depletion. Scale bar, 20μm.

g, Intima rupture in the aortae of Cx3cr1^{creERT2};CSF1R^{lslDTR} 14-days post-continued Mac^{AIR}-depletion. Yellow arrowheads indicate ruptured areas that also showed high concentration of fibrin(ogen) (Fb(g)) deposits. VE-Cadherin identifies endothelial cells in red. Scale bar, 20μm.

h, D-dimer plasma levels in Cx3cr1^{creERT2};CSF1R^{DTR} and littermate control mice 14-days post-macrophage depletion (n=6-13 per group, Mann-Whitney *T*-test, ± SEM, **p ≤ 0.01).

i-j, Kidneys, lung, and liver from sick Cx3cr1^{creERT2};CSF1R^{DTR} mouse 7- or 14-days of macrophage depletion. **i** Note multiple hemorrhagic foci (blue arrow head).

j, Fibrin(ogen) immunohistochemistry on kidney sections of control and Cx3cr1^{creERT2};CSF1R^{DTR} mice. Scale bar, 50μm; n=4-11 per group.

k, Flow cytometry analysis evaluating the percentage of Cx3cr1+Csf1r+CD45+ cells in bone marrow (BM), lung, liver, kidney, and peripheral blood (PB) in control and Cx3cr1^{creERT2};CSF1R^{DTR} mice one day post-diphtheria toxin injection (n=5 per group, Mann-Whitney *T*-test, ± SEM, *p ≤ 0.05, **p ≤ 0.01). Representative flow cytometry plots are below graph.

l, Transcript levels of plasminogen receptors (*Eno1* and *Plgrkt*) in adventitial macrophages and Mac^{AIRs} from scRNA-seq data sets in Supplemental Fig. 2.

m, Experimental design of FITC-conjugated albumin or plasminogen intravenous injection (on the left). Aortae were harvested 4hrs post-injection. On the right: visualization of the experimental outcome in the *en face* aortae. Distribution of intravenously injected FITC-conjugated albumin (control, upper panels) or plasminogen (lower panels) in relation to Mac^{AIRs} (yellow arrow heads) identified by CD45 (white). Endothelial cells were identified by Pecam1 (red). Scale bar, 5μm; n=3 per group.

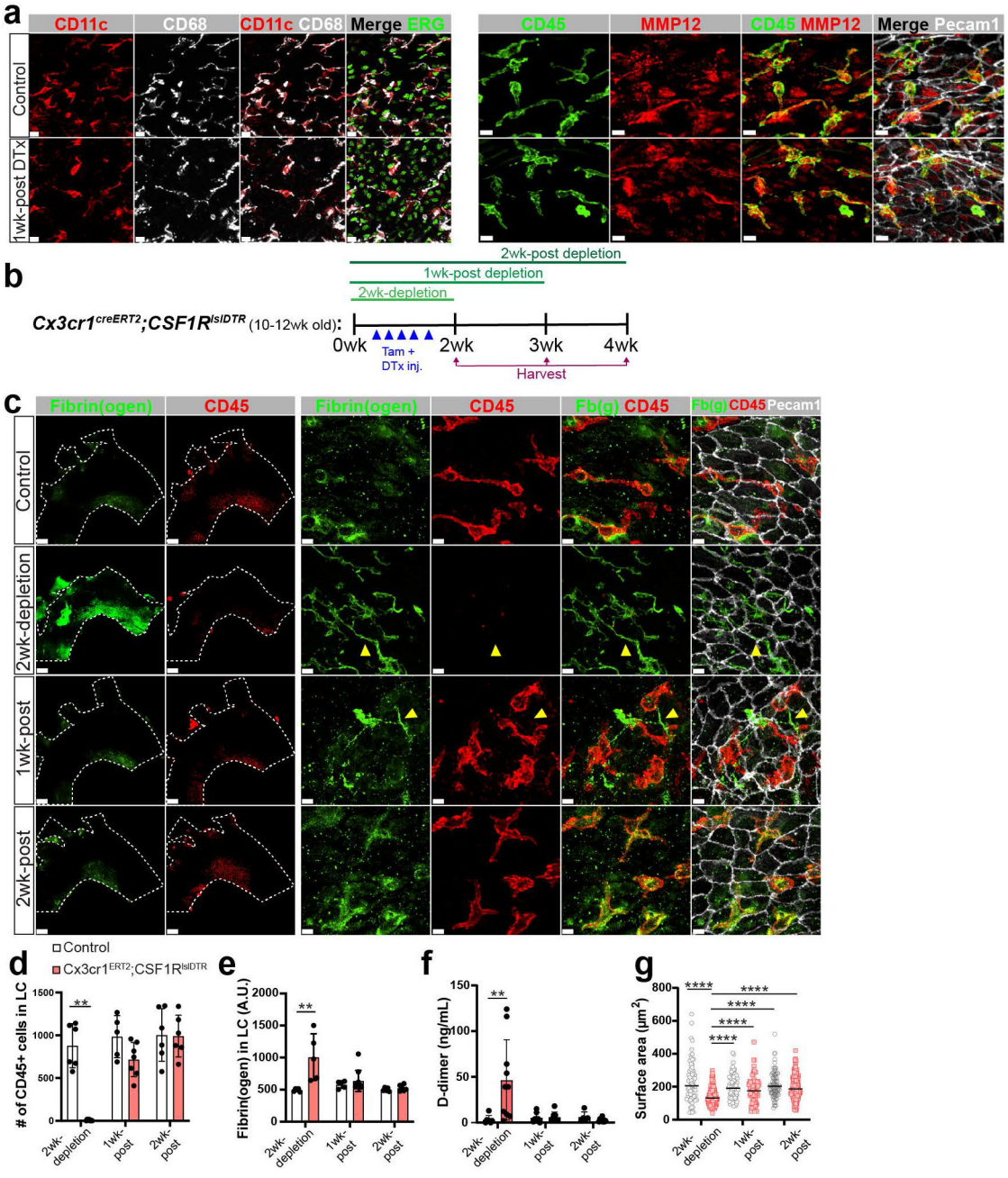

Figure 7. Rescue of the phenotype (fibrin accumulation) upon return of Mac^{AIRs}

a, *En face* images of littermate control and Cx3cr1^{creERT2};CSF1R^{DTR} mice 1-wk after single-diphtheria (DTx) injection. Stopping tamoxifen and DTx injections ceases the pressure of cell ablation and allows for the repopulation of intimal immune cells. Aortae were stained for Mac^{AIR} markers to validate the monocyte-derived population that repopulates the arch after resident population is depleted have the Mac^{AIR} identity (CD11c+MMP12+CD68+CD45+)(n=3; Scale bar, 15μm (left panel) & 10μm (right panel)). **b,** Schematic of macrophage rescue experiments. Littermate control and Cx3cr1^{creERT2};CSF1R^{DTR} mice were both injected with tamoxifen (tam) and diphtheria

toxin (DTx) for 2 weeks of continued macrophage-depletion. After 2weeks, administration of tam and DTx stopped, allowing for Mac^{AIRs} to repopulate the aorta. Aortae *en face* were evaluated at 2wk-depletion (base-line) and after ceasing tam/DTx treatment: 1wk-post depletion (1wk-post), and 2wk post depletion (2wk-post).

c, *En face* images evaluating fibrin(ogen) (green) and Mac^{AIR} (red) accumulation of littermate control and $Cx3cr1^{creERT2}$;$CSF1R^{DTR}$ aortae at the given time-points. Fibrin fibrils are noted by yellow arrow heads. Endothelial cells are identified with VE-Cadherin (white). Scale bar, 300μm, 7μm.

d, Total number of intimal CD45+ cells in the lesser curvature (LC) of the aortic arch in littermate controls and $Cx3cr1^{creERT2}$; $CSF1R^{lslDTR}$ mice at 2wk-depletion, 1wk-post depletion, and 2wk-post depletion (n=5-7 per group, Mann-Whitney *T*-test, ± SD, **p ≤ 0.01).

e, Mean Fluorescence Intensity of Fibrin(ogen) in the lesser curvature of the aortic arch (n= 5-10 per group, Mann-Whitney *T*-test, ± SEM, **p ≤ 0.01).

f, D-dimer plasma levels (n=5-10 per group, Mann-Whitney *T*-test, ± SEM, **p ≤ 0.01).

g, Surface area measurements of endothelial cells in the lesser curvature of $Cx3cr1^{creERT2}$;$CSF1R^{lslDTR}$ and littermate control. (n= 3-4 per group, Mann-Whitney T-test, ± SD, ****p ≤ 0.0001).